J|A|C|S
ARTICLES
Published on Web 04/27/2002

Electron Delocalization in Acyclic and *N*-Heterocyclic Carbenes and Their Complexes: A Combined Experimental and Theoretical Charge-Density Study

Maxim Tafipolsky,[†] Wolfgang Scherer,*[,†] Karl Öfele,[†] Georg Artus,[‡] Bjørn Pedersen,[‡] Wolfgang A. Herrmann,[†] and G. Sean McGrady[§]

Contribution from the Anorganisch-chemisches Institut der Technischen Universität München, Lichtenbergstrasse 4, D-85747 Garching, Germany, Technische Universität München, Neue Forschungs-Neutronenquelle, Lichtenbergstrasse 1, D-85747 Garching, Germany, and Department of Chemistry, King's College London, Strand, London, WC2R 2LS, U.K.

Received July 19, 2001

Abstract: Combined experimental and theoretical charge-density studies on free and metal-coordinated *N*-heterocyclic carbenes have been performed to investigate the extent of electron delocalization in these remarkable species. Tracing the orientation of the major axis of the bond ellipticity (the least negative curvature in the electron density distribution) along the *complete bond paths* distinguishes unambiguously between fully delocalized systems and those with interrupted cyclic electron delocalization. Evaluation of charge-density-based properties such as atomic quadrupole moments serves as a direct and quantitative measure of the extent of π-electron delocalization and reveals consistency between theory and experiment. A detailed topological analysis of theoretical charge densities for two benchmark carbene systems, viz., 1,2-dimethylpyrazol-3-ylidene **1a** and 1,3-dimethylimidazol-2-ylidene **2a**, and their corresponding stable chromium pentacarbonyl complexes **1** and **2**, highlights the advantages of charge-density-based criteria to analyze such complex electronic situations. Thus, **1a** and **2a** display a different extent of electron delocalization; yet nearly identical p_π occupations at the carbene center are computed for **1a** and **2a**. However, atomic quadrupoles Q_{zz} − the charge-density analogues of p_π occupation − reveal faithfully the electronic differences in **1a** and **2a** and demonstrate the sensitivity of charge-density-based properties to the bonding situation. The acyclic aminocarbene $(i\mathrm{Pr}_2\mathrm{N})_2\mathrm{CCr(CO)}_4$ has also been studied, and the high barrier to rotation about the C−N bond is shown not to arise solely from p_π−p_π bonding.

1. Introduction

Organometallic carbene complexes play an increasingly important role as intermediates in homogeneous catalysis in reactions such as alkene metathesis, Fischer−Tropsch synthesis, alkene and alkyne polymerization, and cyclopropanation.[1] Recently, *N*-heterocyclic carbenes have been used to complement and extend the capabilities of the ubiquitous phosphane ligands.[2] Much of the interest in *N*-heterocyclic carbenes derives from the advantages they impute as ligands in organometallic catalysts, where they broaden the scope of applications accessible to phosphanes. Additionally, they are less sensitive to air and moisture, as compared to their phosphane counterparts, and have proved remarkably resistant to oxidation,[2c] with phosphane degradation through C−P bond cleavage being rather facile in comparison.

As early as the 1960s, Wanzlick[3] and Öfele[4] described *N*-heterocyclic metal-carbene complexes obtained from imidazolium salts. Subsequently, almost two decades passed before Arduengo et al. succeeded in isolating a free imidazol-2-ylidene.[5] This success stimulated a plethora of experimental and theoretical studies into the structure and properties of these unexpectedly stable nucleophilic carbenes, which can be handled

* To whom correspondence should be addressed. Fax: +49 89 289 13473. E-mail: Wolfgang.Scherer@ch.tum.de.
[†] Anorganisch-chemisches Institut der Technischen Universität München.
[‡] Technische Universität München.
[§] King's College London.

(1) For general reviews, see: (a) Herrmann, W. A.; Köcher, C. *Angew. Chem.* **1997**, *109*, 2256−2282; *Angew. Chem., Int. Ed. Engl.* **1997**, *36*, 2162−2187. (b) Weskamp, T.; Böhm, V. P. W.; Herrmann, W. A. *J. Organomet. Chem.* **2000**, *600*, 12−22. (c) Bourissou, D.; Guerret, O.; Gabbaï, F. P.; Bertrand, G. *Chem. Rev.* **2000**, *100*, 39−91. (d) Herrmann, W. A. *Angew. Chem., Int. Ed.* **2002**, *41*, 1290−1309.

(2) (a) Herrmann, W. A.; Köcher, C.; Gooen, L. J.; Artus, G. R. *Chem.-Eur. J.* **1996**, *2*, 1627−1636. (b) Herrmann, W. A.; Elison, M.; Fischer, J.; Köcher, C.; Artus, G. R. *Angew. Chem.* **1995**, *107*, 2602−2605; *Angew. Chem., Int. Ed. Engl.* **1995**, *34*, 2371−2374. (c) Herrmann, W. A.; Roesky, P. W.; Elison, M.; Artus, G. R.; Öfele, K. *Organometallics* **1995**, *14*, 1085−1086. (d) Herrmann, W. A.; Gooen, L. J.; Köcher, C.; Artus, G. R. *Angew. Chem.* **1996**, *108*, 2980−2982; *Angew. Chem., Int. Ed. Engl.* **1996**, *35*, 2805−2807. (e) Weskamp, T.; Schattenmann, W. C.; Spiegler, M.; Herrmann, W. A. *Angew. Chem.* **1998**, *110*, 2631−2633; *Angew. Chem., Int. Ed.* **1998**, *37*, 2490−2493. (f) Weskamp, T.; Kohl, F. J.; Hieringer, W.; Gleich, D.; Herrmann, W. A. *Angew. Chem.* **1999**, *111*, 2573−2576; *Angew. Chem., Int. Ed.* **1999**, *38*, 2416−2419. (g) Frenzel, U.; Weskamp, T.; Kohl, F. J.; Schattenmann, W. C.; Nuyken, O.; Herrmann, W. A. *J. Organomet. Chem.* **1999**, *586*, 263−265. (h) Ackermann, L.; Fürstner, A.; Weskamp, T.; Kohl, F. J.; Herrmann, W. A. *Tetrahedron Lett.* **1999**, *40*, 4787−4790.

(3) Wanzlick, H.-W., Schönherr, H.-J. *Angew. Chem.* **1968**, *80*, 154−155; *Angew. Chem., Int. Ed. Engl.* **1968**, *7*, 141−142.

(4) Öfele, K. *J. Organomet. Chem.* **1968**, *12*, P42−P43.

(5) Arduengo, A. J., III. *Acc. Chem. Res.* **1999**, *32*, 913−921 and references therein.

under an inert atmosphere even at ambient temperatures. To date, a variety of stable *N*-heterocyclic carbenes − both saturated and unsaturated − along with silylene[6] and germylene[7] analogues have been synthesized. Recently, 1,3,4-triphenyl-4,5-dihydro-1*H*-1,2,4-triazol-5-ylidene has been isolated and structurally characterized and is commercially available,[8] and the first acyclic species − bis(diisopropylamino)carbene − was prepared and characterized by a single-crystal X-ray diffraction study.[9]

N,*N*′-heterocyclic carbenes have a singlet (σ^2) electronic ground state. The $-I$ effect of the N atoms induces a large $\sigma-p_\pi$ gap by stabilizing the nonbonding σ orbital while leaving the p_π orbital energetically unchanged. Additional mesomeric stabilization of the heterocyclic carbene by the lone pairs at the N substituents results formally in a three-center, four-electron π-system. Hence, a combination of inductive (σ-acceptor) and mesomeric (π-donor) effects formally preserves the electronic neutrality of the carbene center by an electronic pull-push mechanism. A common feature is the presence of two π-donor substituents, of which at least one is an amino group.[10] However, there are more subtle effects at work in the bonding of *N*-heterocyclic carbenes (qv). Their remarkable stability has been explored by several theoretical studies, with two contrary bonding descriptions having been advanced: (i) On the basis of ab initio calculations, Cioslowski considered the stability of the simple 1,3-dimethylimidazol-2-ylidene carbene to derive almost exclusively from substantial σ-charge transfer from the carbenic C atom to the more electronegative neighboring N atoms; π-donation was found to play only a minor role.[11a] This conclusion was supported simultaneously by further calculations,[11b,d] PE spectroscopy,[11c] a combined neutron/X-ray charge-density study on 1,3,4,5-tetramethylimidazol-2-ylidene-d12,[11b] and an X-ray study on 1,3-di-1-adamantylimidazol-2-ylidene.[11k] (ii) On the basis of a natural population analysis (NPA),[12a,b] Frenking et al.[11e] argued that the stabilization arises primarily from π-donation by the lone pairs of the N atoms into the formally empty p_π orbital of the carbenic C atom; these authors suggested that cyclic electron delocalization in imidazol-2-ylidenes is significant and displays some aromatic character, a conclusion supported by inner-shell electron-energy loss spectroscopy[11g] and a further theoretical study by Heinemann et al.[11f] Cyclic electron stabilization was estimated at ca. 25 kcal mol^{-1}. Frenking et al.[11e] showed the unsaturated (6π) cyclic *N*,*N*′-aminocarbenes to be more stable than their saturated (4π) counterparts, but reported that the degree of conjugation and aromaticity depends on the criteria used and the reference system employed.[11f] The "atoms-in-molecules" (AIM) method, based on topological analysis of the charge density,[13] revealed the aromatic character to be weak, with it being more pronounced with regard to energetic and magnetic properties.[14]

To ascertain the role and extent of aromatic stabilization in *N*-heterocyclic carbenes, we have performed both experimental and theoretical charge-density studies on two benchmark carbene systems, viz., 1,2-dimethylpyrazol-3-ylidene **1a** and 1,3-dimethylimidazol-2-ylidene **2a**, on their corresponding stable chromium pentacarbonyl complexes **1** and **2**,[4] and on several related model systems including other carbene-transition metal complexes. Whereas **2a** exists as a stable species, the free carbene **1a** has not yet been reported. The greater tractability of **2a** might derive solely from inductive effects, since the carbene center in **1a** is attached to just one electron-withdrawing N atom as opposed to two in **2a**. In contrast, *both* pentacarbonyl complexes **1** and **2** display a remarkable stability which may arise from enhanced electronic delocalization.

In this study, we have analyzed the *topology of the total charge density and its Laplacian*, obtained by combined experimental and theoretical studies on the basis of the AIM method.[13] Hence, we have gained a deeper insight into the nature of the metal-carbene bond and the delocalized π-bonding in the heterocyclic ring. First, we introduce a new and sensitive measure for the degree of electron delocalization in *N*-heterocyclic carbenes. Second, we analyze for the first time the effects of carbene coordination with respect to core polarization at the metal center, and the nucleophilic or electrophilic nature of the carbene C atom on the basis of experimental charge densities. Third, we demonstrate that even those topological parameters which depend on very subtle features of the charge density, such as atomic quadrupoles or the orientation of the major axis of the bond ellipticity along a complete bond path, may be obtained from precise high-resolution X-ray data in good agreement with theoretical calculations.[15]

2. Results and Discussion

2.1. Molecular Structure of Carbenes 1a and 2a and Their Chromium Pentacarbonyl Complexes 1 and 2. For complex **1** we employed a CCD detector system in combination with a rotating anode to obtain low-temperature high-resolution X-ray data ($\sin\theta_{max}/\lambda = 1.09$ Å^{-1}; $T = 100$ K) of sufficient quality for a topological analysis[13] of the experimental charge density.

(6) Denk, M.; Lennon, R.; Hayashi, R.; West, R.; Belyakov, A. V.; Verne, H.-P.; Haaland, A.; Wagner, M.; Metzler, N. *J. Am. Chem. Soc.* **1994**, *116*, 2691−2692.
(7) Herrmann, W. A.; Denk, M.; Behm, J.; Scherer, W.; Klingan, F.-R.; Bock, H.; Solouki, B.; Wagner, M. *Angew. Chem.* **1992**, *104*, 1489−1492; *Angew. Chem., Int. Ed. Engl.* **1992**, *31*, 1485−1488.
(8) Enders, D.; Breuer, K.; Raabe, G.; Runsink, J.; Teles, J. H.; Melder, J.-P.; Ebel, K.; Brode, S. *Angew. Chem.* **1995**, *107*, 1119−1122; *Angew. Chem., Int. Ed. Engl.* **1995**, *34*, 1021−1023.
(9) Alder, R. W.; Allen, P. R.; Murray, M.; Orpen, A. G. *Angew. Chem.* **1996**, *108*, 1211−1213; *Angew. Chem., Int. Ed. Engl.* **1996**, *35*, 1121−1123.
(10) We note that no stable dialkoxycarbene has yet been reported. This may be related to the superior π-donor capabilities of amino versus alkoxy ligands. For details of ab initio studies, see: (a) Sauers, R. R. *Tetrahedron Lett.* **1996**, *37*, 149−152. (b) Sauers, R. R. *Tetrahedron Lett.* **1994**, *35*, 7213−7216. For stable aminooxy- and aminothiocarbenes, see: Alder, W. R.; Butts, C. P.; Orpen, A. G. *J. Am. Chem. Soc.* **1998**, *120*, 11526−11527.
(11) (a) Cioslowski, J. *Int. J. Quantum Chem., Quantum Chem. Symp.* **1993**, *27*, 309−319. (b) Arduengo, A. J., III; Dias, H. V. R.; Dixon, D. A.; Harlow, L. R.; Klooster, W. T.; Koetzle, T. F. *J. Am. Chem. Soc.* **1994**, *116*, 6812−6822. (c) Arduengo, A. J., III; Bock, H.; Chen, H.; Denk, M.; Dixon, D. A.; Green, J. C.; Herrmann, W. A.; Jones, N. L.; Wagner, M.; West, R. *J. Am. Chem. Soc.* **1994**, *116*, 6641−6649. (d) Arduengo, A. J., III; Dixon, D. A.; Kumashiro, K. K.; Lee, C.; Power, W. P.; Zilm, K. W. *J. Am. Chem. Soc.* **1994**, *116*, 6361−6367. (e) Boehme, C.; Frenking, G. *J. Am. Chem. Soc.* **1996**, *118*, 2039−2046. (f) Heinemann, C.; Müller, T.; Apeloig, Y.; Schwarz, H. *J. Am. Chem. Soc.* **1996**, *118*, 2023−2038. (g) Lehmann, J. F.; Urquhart, S. G.; Ennis, L. E.; Hitchcock, A. P.; Hatano, K.; Gupta, S.; Denk, M. K. *Organometallics* **1999**, *18*, 1862−1872. (h) Heinemann, C.; Thiel, W. *Chem. Phys. Lett.* **1994**, *217*, 11−16. (i) Heinemann, C.; Herrmann, W. A.; Thiel, W. *J. Organomet. Chem.* **1994**, *475*, 73−84. (j) Dixon, D. A.; Arduengo, A. J., III. *J. Phys. Chem.* **1991**, *95*, 4180−4182. (k) Arduengo, A. J., III; Harlow, L. R.; Kline, M. *J. Am. Chem. Soc.* **1991**, *113*, 361−363.
(12) (a) Reed, A. E.; Weinstock, R. B.; Weinhold, F. *J. Chem. Phys.* **1985**, *83*, 735−746. (b) Reed, A. E.; Curtiss, L. A.; Weinhold, F. *Chem. Rev.* **1988**, *88*, 899−926. (c) Gaussian NBO Version 3.1; see ref 76.
(13) Bader, R. F. W. *Atoms in Molecules − A Quantum Theory*; Oxford University Press: Oxford, U.K., 1990.
(14) The topology of the charge-density distribution was analyzed at the HF/6-31G(d) level (see ref 11f), which may be insufficient to describe the electronic situation in delocalized systems. Indeed, our results show that inclusion of electron correlation is critical for a comparative study of the charge-density distributions in *N*-heterocyclic carbenes; see also: (a) Boyd, R. J.; Wang, L.-C. *J. Comput. Chem.* **1989**, *10*, 367−375. (b) Laidig, K. E. *Chem. Phys. Lett.* **1994**, *225*, 285−292.

Table 1. Topological Parameters at the BCP of Experimental and Theoretical Charge Densities for **1**[a]

	r(A–B), [Å]	$\rho(\mathbf{r}_c)$, [e Å^{-3}]	$\nabla^2\rho(\mathbf{r}_c)$, [e Å^{-5}]	ϵ		r(A–B), [Å]	$\rho(\mathbf{r}_c)$, [e Å^{-3}]	$\nabla^2\rho(\mathbf{r}_c)$, [e Å^{-5}]	ϵ
Cr−C_{carb}					C_{carb}−N				
exp	2.1327(4)	0.543(6)	6.113(7)	0.08	exp	1.3568(5)	2.00(2)	−12.88(8)	0.24
calc	2.120 (2.130)	0.52 (0.52)	6.7 (6.0)	0.04 (0.05)	calc	1.374 (1.370)	1.91 (1.96)	−9.1 (−10.4)	0.06 (0.06)
Cr−CO ax					N−N				
exp	1.8557(4)	0.86(1)	12.24(2)	0.03	exp	1.3711(5)	2.31(2)	−4.46(8)	0.26
calc	1.868 (1.876)	0.82 (0.81)	13.5 (12.0)	0.04 (0.03)	calc	1.395 (1.392)	2.19 (2.24)	−13.7 (−12.4)	0.25 (0.24)
Cr−CO eq[b]					N−C(=C)				
exp	1.8971(2)	0.734(2)	11.149(3)	0.08	exp	1.3409(7)	2.21(2)	−21.3(1)	0.06
calc	1.891 (1.898)	0.76 (0.76)	13.2 (11.7)	0.07 (0.06)	calc	1.362 (1.358)	2.02 (2.07)	−12.7 (−13.9)	0.20 (0.16)
C−O ax					C=C				
exp	1.159(1)	3.15(3)	−3.5(2)	0.02	exp	1.3803(8)	2.16(2)	−19.50(6)	0.27
calc	1.179 (1.163)	2.78 (3.03)	21.3 (6.1)	0.00 (0.00)	calc	1.387 (1.380)	2.05 (2.09)	−18.8 (−19.9)	0.30 (0.26)
C−O eq[b]					C_{carb}−C				
exp	1.1483(3)	3.20(1)	−1.93(6)	0.04	exp	1.4198(5)	1.94(2)	−14.86(4)	0.09
calc	1.177 (1.161)	2.79 (3.04)	22.0 (6.5)	0.01 (0.00)	calc	1.432 (1.428)	1.92 (1.95)	−17.2 (−17.4)	0.18 (0.17)

[a] BPW91/I level (corresponding values at the BPW91/II level of theory are given in parentheses). [b] Average value.

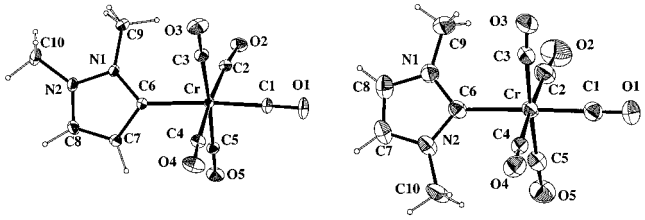

Figure 1. Molecular X-ray structure of **1** at $T = 100$ K (left) and **2** at $T = 173$ K (right): atomic displacement ellipsoids for non-H atoms are drawn at the 50% probability level; only one of the two independent molecules of **2** is shown. Selected bond distances [Å] and angles [deg] for **1**: Cr−C1 1.8557(4), Cr−C2 1.8905(4), Cr−C3 1.9104(4), Cr−C4 1.9058(4), Cr−C5 1.8816(4), Cr−C6 2.1327(4), C1−O1 1.159(1), C2−O2 1.1522(6), C3−O3 1.1445(7), C4−O4 1.1458(7), C5−O5 1.1509(7), N1−N2 1.3711(5), N1−C6 1.3568(5), N1−C9 1.4514(6), N2−C8 1.3409(7), N2−C10 1.4555(5), C6−C7 1.4198(5), C7−C8 1.3803(8), ∠N1−C6−C7 104.02(3), ∠C6−C7−C8 108.47(4), ∠C7−C8−N2 108.48(4), ∠C8−N2−N1 107.41(4), ∠N2−N1−C6 111.61(3). For **2** (parameters for the second independent molecule are in square brackets): Cr−C1 1.867(2) [1.869(2)], Cr−C2 1.909(2) [1.908(2)], Cr−C3 1.908(2) [1.901(2)], Cr−C4 1.879(2) [1.891(2)], Cr−C5 1.893(2) [1.895(2)], Cr−C6 2.138(2) [2.145(2)], C1−O1 1.147(3) [1.145(2)], C2−O2 1.139(2) [1.141(2)], C3−O3 1.147(3) [1.146(2)], C4−O4 1.149(3) [1.144(3)], C5−O5 1.149(3) [1.141(3)], N1−C6 1.364(2) [1.364(2)], N1−C8 1.385(2) [1.385(3)], N1−C9 1.455(3) [1.453(3)], N2−C6 1.367(2) [1.368(2)], N2−C7 1.381(2) [1.387(2)], N2−C10 1.460(3) [1.454(3)], C7−C8 1.331(3) [1.330(3)], ∠N1−C6−N2 102.7(1) [102.6(2)], ∠C6−N2−C7 111.8(2) [112.0(2)], ∠N2−C7−C8 107.0(2) [106.5(2)], ∠C7−C8−N1 106.6(2) [107.2(2)], ∠C8−N1−C6 111.9(2) [111.8(2)].

In addition, a conventional X-ray study of **2** and tetracarbonyl{bis(diisopropylamino)carbene}chromium, **10**, was performed. The geometrical parameters deduced from both studies are in good agreement with DFT calculations at the BPW91/I and BPW91/II level of theory. Salient experimental and calculated distances and angles are listed in Table 1, and the structures are depicted in Figures 1 and 2. Unless otherwise stated, our standard theoretical model is based on DFT calculations at the BPW91/I level of theory.

σ-Donor/π-Acceptor Capabilities. The σ-donor/π-acceptor capacity of a ligand L is often quantified by coordination to a metal carbonyl fragment and measurement of the M−L distance and the trans ν(CO) vibrational frequencies. The Cr−C(carbene) bond distance of **1** [2.1327(4) Å] is only marginally shorter than that in **2** [2.138(2) and 2.145(2) Å; two independent molecules], in agreement with the calculated values of 2.120 and 2.134 Å for **1** and **2**, respectively. These bond parameters compare well with the related complexes (μ^2-4,5-dioxy-1,3-dimethylimidazolin-2-ylidene)-dioxo-dipyridyl-osmium(VI)-pentacarbonyl-chromium(0),[2c] **3** [r(Cr−C) = 2.129(4) Å], and *cis*-tetracarbonyl-bis(1,3-dimethylimidazol-2-ylidene)-chromium,[16] **4** [r(Cr−C) = 2.131(3) Å] (Scheme 1). The Cr−C(carbene) bond distance in these complexes is diagnostic of the nature of the carbene ligand, being strongly influenced by its σ-donor and π-acceptor characteristics. Thus, bis(2,4,6-trimethylphenyl)bis(1,3-diisopropyl-4,5-dimethylimidazol-2-ylidene)chromium, **5**,[17] displays a significantly longer Cr−C(carbene) bond [2.175(3) Å].[18,19]

Fischer-type carbenes [C(X)R with X = OR, SR; R = alkyl] display rather short Cr−C(carbene) bond distances, indicating substantial π back-donation from the metal (see Scheme 2, structure II). Replacement of X by a better π-donor lengthens the Cr−C(carbene) bond substantially and shortens the C−X bond (structure III).

By analogy, **1a** might be classified as a better π-acceptor ligand than **2a**. However, neither experimental nor calculated Cr−C(carbene) bond distances differ significantly between **1** and **2**, and the calculated trans ν(CO) frequencies reveal the *opposite* trend: ν(CO) for **1** is less than that for **2** (1933 vs 1936 cm^{-1}, respectively).[19] Hence, the anticipated σ-donor/π-acceptor properties of **1a** and **2a** do not reveal themselves on complexation either on the basis of geometrical criteria or from interpretation of trans ν(CO) frequencies.

(15) Despite the importance of the *experimental* electron density to an understanding of transition-metal chemistry, only a few organometallic compounds have been investigated by high-resolution X-ray diffraction to date; see: (a) Macchi, P.; Proserpio, D. M.; Sironi, A. *J. Am. Chem. Soc.* **1998**, *120*, 1447−1455. (b) Macchi, P.; Proserpio, D. M.; Sironi, A. *J. Am. Chem. Soc.* **1998**, *120*, 13429−13435. (c) Scherer, W.; Hieringer, W.; Spiegler, M.; Sirsch, P.; McGrady, G. S.; Downs, A. J.; Haaland, A.; Pedersen, B. *J. Chem. Soc., Chem. Commun.* **1998**, 2471−2472. (d) Iversen, B. B.; Larsen, F. K.; Figgis, B. N.; Reynolds, P. A. *J. Chem. Soc., Dalton Trans.* **1997**, 2227−2240. (e) Macchi, P.; Schultz, A. J.; Larsen, F. K.; Iversen, B. B. *J. Phys. Chem.* **2001**, *A105*, 9231−9242. Only one study on the electron distribution in Fischer-type carbenes exploring both *experimental* and *theoretical* charge densities has been published; see: Wang, C.-C.; Wang, Y.; Liu, H.-J.; Lin, K.-J.; Chou, L.-K.; Chan, K.-S. *J. Phys. Chem.* **1997**, *A101*, 8887−8901.

(16) Ackermann, K.; Hofmann, P.; Köhler, F. H.; Kratzer, H.; Krist, H.; Öfele, K.; Schmidt, H. R. *Z. Naturforsch.* **1983**, *B38*, 1313−1324.

(17) Danopoulos, A. A.; Hankin, D. M.; Wilkinson, G.; Cafferkey, S. M.; Sweet, T. K. N.; Hursthouse, M. B. *Polyhedron* **1997**, *16*, 3879−3892.

(18) The rather short Cr−C(carbene) distances observed for **1** and **2** versus **5** might indicate some π-acceptor capacity in *N,N′*-heterocyclic carbenes despite their general classification as pure σ-donor ligands; see ref 19.

(19) In many studies the σ-donor/π-acceptor properties of the carbene ligands are characterized by comparing the values of the ν(CO) vibrational frequency in a metal carbonyl which is trans to the carbene ligand; a lower frequency correlates with reduced π-acceptor character of the carbene ligand. On account of the symmetry in **2** (C_2), the individual ν(CO) modes could not be resolved in the experimental spectrum; thus we have based our discussion on calculated frequencies alone.

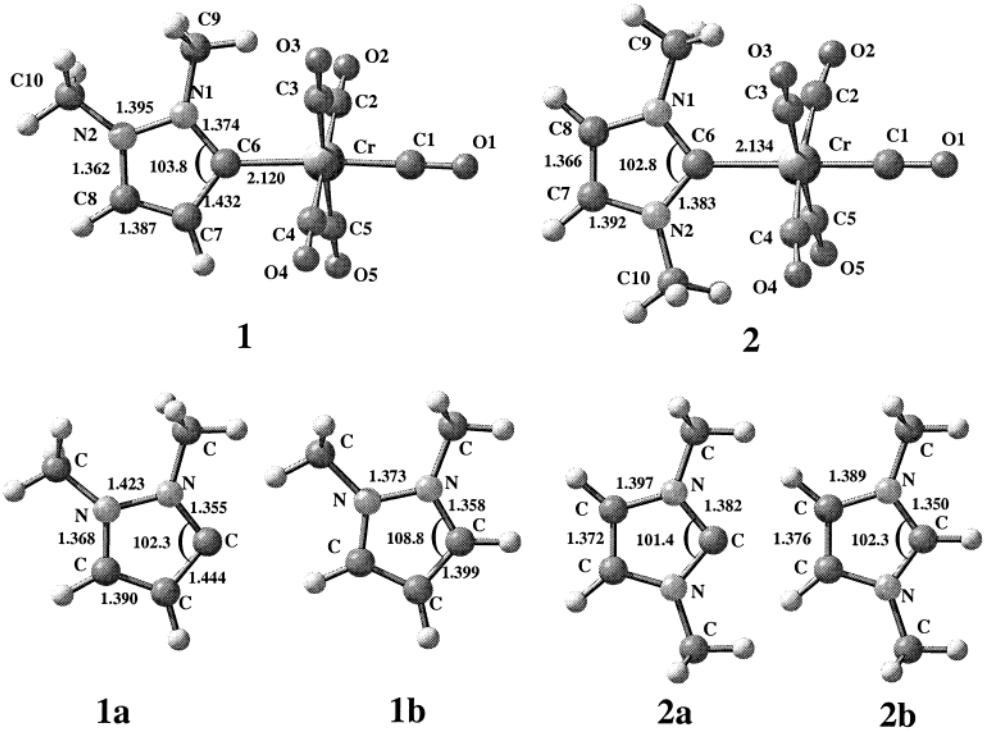

Figure 2. Optimized geometries at the BPW91/I level of theory for **1**, **2**, **1a**, **2a**, **1b**, and **2b**. Bond distances are given in Å, and angles are given in deg.

Geometry of the *N*-Heterocyclic Rings. The calculated bond distances in the five-membered ring of carbene **2a** do not change significantly on coordination to $Cr(CO)_5$ (Figure 2): $C_{carb}-N$ = 1.382 (1.383) Å; N−C = 1.397 (1.392) Å; C═C = 1.372 (1.366) Å for **2a** and **2**, respectively. This is inconsistent with a σ-only $M-C_{carb}$ interaction, which should shorten the $C_{carb}-N$ bonds on coordination to $M(CO)_5$ fragments.[22e] In the case of **1a** and **1**, an *elongation* of the $C_{carb}-N$ bond in fact attends coordination to the $M(CO)_5$ fragment ($C_{carb}-N$ = 1.355 and 1.374 Å, for **1a** and **1**, respectively).[20] Thus, the $C_{carb}-N$ bonds within the five-membered heterocycles of **1** and **2** are unique in deviating from the trend outlined above, displaying distances slightly greater in complexes **1** and **2** than in the corresponding free carbenes **1a** and **2a** and in the pyrazolium (**1b**) and imidazolium (**2b**) cations, which were included in our study as representative π-delocalized systems (Figure 2). The $C_{carb}-N$ bonds seem to play a pivotal role in the bonding of these benchmark compounds. These remarkable structural features should be also reflected in the topology of the charge density. Accordingly, we investigated their nature by further theoretical calculations and a detailed topological analysis of the charge density, as described in the next sections.

Table 2. Results of the Natural Population Analysis at the BPW91/I Level

compound	$p_\pi(C_{carb})$[a]	$q(C_{carb})$[b]	q(N)
1	0.80	0.02	−0.18[c]
1a	0.65	−0.08	−0.22[c]
2	0.79	0.24	−0.37
2a	0.66	0.08	−0.40

bond	Wiberg bond index
1 (**1a**)[d]	
$Cr-C(O)_{ax}$	0.95[e]
$Cr-C(O)_{eq}$ (av)	0.83[e]
$Cr{=}C_{carb}$	0.46[e]
C−O (av)	2.0[e]
$C_{carb}-N$	1.36 (1.25)
N−N	1.04 (0.97)
N−C	1.23 (1.22)
C═C	1.52 (1.55)
$C_{carb}-C$	1.34 (1.33)
2 (**2a**)[d]	
$C_{carb}-N$	1.23 (1.25)
N−C	1.12 (1.11)
C═C	1.64 (1.64)

[a] Occupation of the p_π orbital at the carbenic C atom (in electrons). [b] Natural charge on the carbenic C atom. [c] Natural charge on the N atom adjacent to the carbenic C atom. [d] Wiberg bond indices for the corresponding free carbenes are given in parentheses. [e] Values were found to be identical for **1** and **2**.

2.2. Interpretation of the Wave Function. Natural Population Analysis (NPA). Table 2 compares the results of the NPA[12c] for carbenes **1a** and **2a** and their corresponding complexes **1** and **2**. The calculated occupancy,[21] $p_\pi(C_{carb})$ = 0.66 e, and the net charge of the carbenic carbon atom, $q(C_{carb})$ = 0.08 e, in **2a** compare well with those obtained at the MP2/6-31G(d) level by Frenking et al.[11e] for the N-unsubstituted imidazol-2-ylidene [$p_\pi(C_{carb})$ = 0.67 e and $q(C_{carb})$ = 0.06 e]. In contrast, only a small negative net charge is found for the carbenic C atom (−0.08) in **1a**, yet the occupancy, $p_\pi(C_{carb})$ =

(20) An X-ray diffraction study (Artus, G. R. J. Ph.D. Thesis, Technical University of Munich, 1996) of a series of Arduengo-type $W(CO)_5$-L carbene complexes (L = *N*,*N*′-heterocyclic carbene ligand) also revealed only an insignificant shortening of the $C_{carb}-N$ bond distance [average $r(C_{carb}-N)$ = 1.364 Å] in comparison with 1,3,4,5-tetramethylimidazol-2−ylidene which is our experimental benchmark compound for a free carbene ligand [$r(C_{carb}-N)$ = 1.367(1) Å; neutron diffraction data from ref 11b].

(21) $p_\pi(C_{carb})$ gives the occupation of the p_π atomic orbital at the carbene carbon; this is assumed to be oriented perpendicular to the ring.

(22) (a) Nakatsuji, H.; Ushio, J.; Han, S.; Yonezawa, T. *J. Am. Chem. Soc.* **1983**, *105*, 426−434. (b) Taylor, T. E.; Hall, M. B. *J. Am. Chem. Soc.* **1984**, *106*, 1576−1584. (c) Jacobsen, H.; Ziegler, T. *Organometallics* **1995**, *14*, 224−230. (d) Vyboishchikov, S. F.; Frenking, G. *Chem.-Eur. J.* **1998**, *4*, 1428−1438. (e) Boehme, C.; Frenking, G. *Organometallics* **1998**, *17*, 5801−5809.

Scheme 1

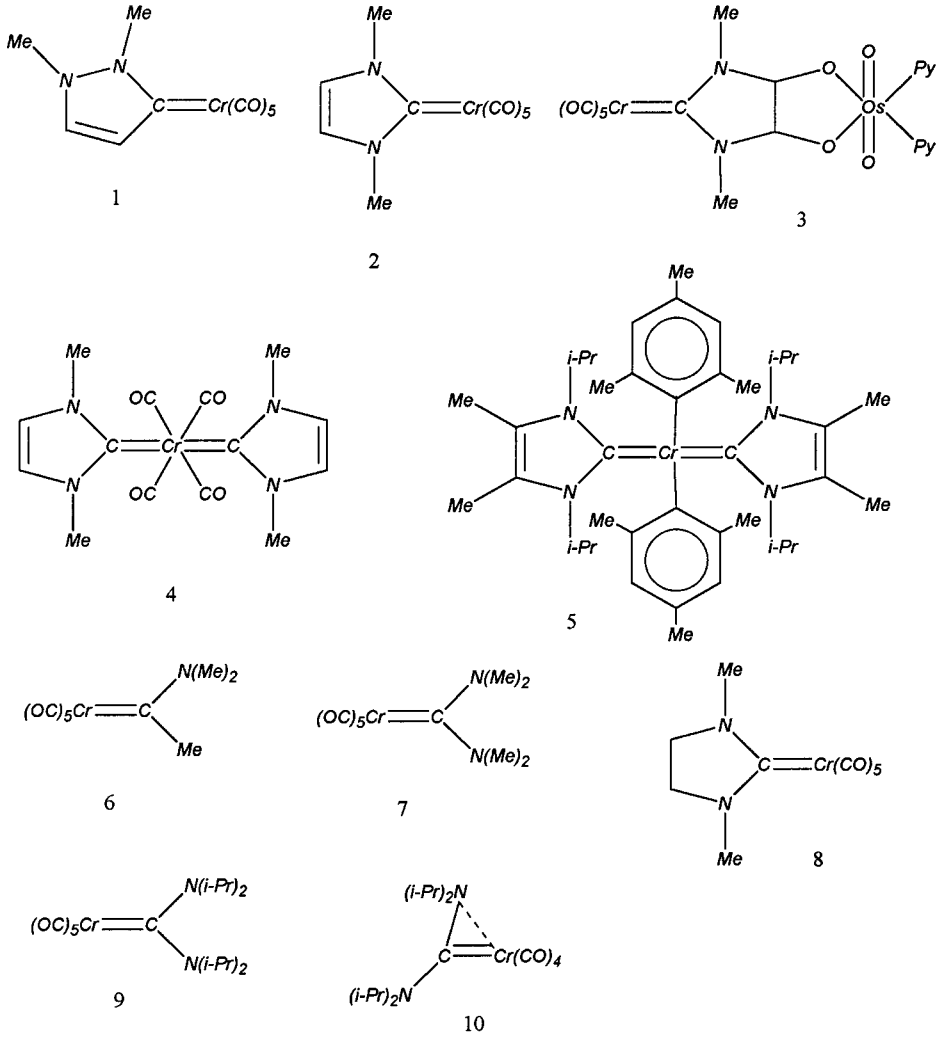

0.65 e, is almost the same as for **2a**. Hence, $p_\pi(C_{carb})$ increases on complexation, but differs only marginally for **1** and **2** (0.80 and 0.79, respectively). A similar effect was observed in a theoretical study of M−Cl (M = Cu, Ag, Au) complexes by Frenking et al.[22e] The NPA results reveal that the net charge on the carbenic C atoms in **1** and **2** becomes more positive and that on the adjacent N atoms becomes less negative on complexation (see Table 2), consistent with significant σ-donation from the ring to the $Cr(CO)_5$ fragment in **1** and **2**. It is noteworthy that the NPA yields a *negative* net charge for the Cr atom (ca. −0.6), both in complexes **1** and **2** and in $Cr(CO)_6$. This is in accord with the results from the NPA of Morokuma et al.,[23] where the *negative* net atomic charge for a transition metal has also been observed. It is interesting also to compare the above results with those obtained for the saturated analogue of **2**, viz., **8**. For **8**, $p_\pi(C_{carb}) = 0.69$ e, smaller than that for **2** (0.79 e). On the basis of the NPA it might be concluded that aminocarbenes are strong σ-donor and weak π-acceptor ligands.

Scheme 2

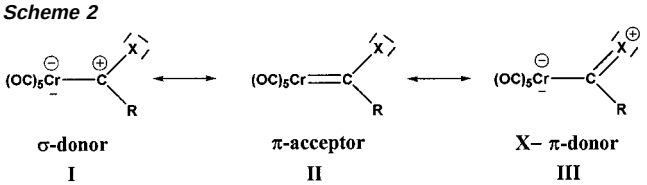

However, since almost identical p_π(carbene) occupations are computed for the free ligands **1a** and **2a** and their corresponding carbene complexes **1** and **2**, respectively, this simple yardstick is too insensitive to the nature of the bonding at the carbene centers in our benchmark systems.

Wiberg Bond Indices. We have attempted an analysis of our systems on the basis of Wiberg bond indices (Table 2). These provide evidence for charge redistribution in the pyrazol-3-ylidene ring in **1** as compared to the free carbene **1a**, whereas the corresponding values for the imidazol-2-ylidene ring in **2** and **2a** are almost identical. Table 2 shows that the indices for the axial and equatorial Cr−(CO) bonds are significantly different in **1**, with the axial ligand being characterized by a larger value and revealing a trans influence for the carbene ligand in **1** and **2**.[24−29] For the saturated analogue of **2**, viz., **8**, calculated Wiberg bond indices for the C_{carb}−N, N−C, and C−C bonds are 1.27, 0.94, and 1.02, respectively.

2.3. Topological Analysis of the Charge Density. In this section, we demonstrate that the electronic nature of free and coordinated carbene ligands is reliably revealed by topological analysis of the charge density. In Table 1, the results of a topological analysis of experimental and theoretical charge densities of **1** are compared. The following salient parameters

(23) Maseras, F.; Morokuma, K. *Chem. Phys. Lett.* **1992**, *195*, 500−504.

at the bond critical points (BCPs) are listed: charge density $\rho(\mathbf{r}_c)$, Laplacian of the charge density $\nabla^2\rho(\mathbf{r}_c)$, and bond ellipticity ($\epsilon$); the electronic kinetic energy density, $G(\mathbf{r}_c)$, and total electronic energy density, $H(\mathbf{r}_c)$, are listed in the Supporting Information.[30,31] All structural and *local* topological parameters from the theoretical calculations are in good agreement with those obtained experimentally. However, the theoretical values derived from the BPW91 calculations using the more flexible basis set II (triple-ζ quality) rather than I (double-ζ quality) lie closer to the experimental values, highlighting the dependence of accuracy on the level of theory employed (qv).[32] Because experimental values are available only for benchmark system **1**, the following discussion of topological features is based on the theoretical calculations unless specified otherwise.

Atomic Basins. Figure 3 depicts the Laplacian of the experimental and theoretical electron density $\nabla^2\rho(\mathbf{r}_c)$ for **1** (a, b) and **2** (c) projected onto the $N-C_{carb}-C$ (**1**) and $N-C_{carb}-N$ (**2**) planes of the *N*-heterocyclic ring. Inspection of the bond paths,[33,34] the location of the BCPs, and the sizes and shapes of the atomic basins[35] clearly reveal the different electronic natures

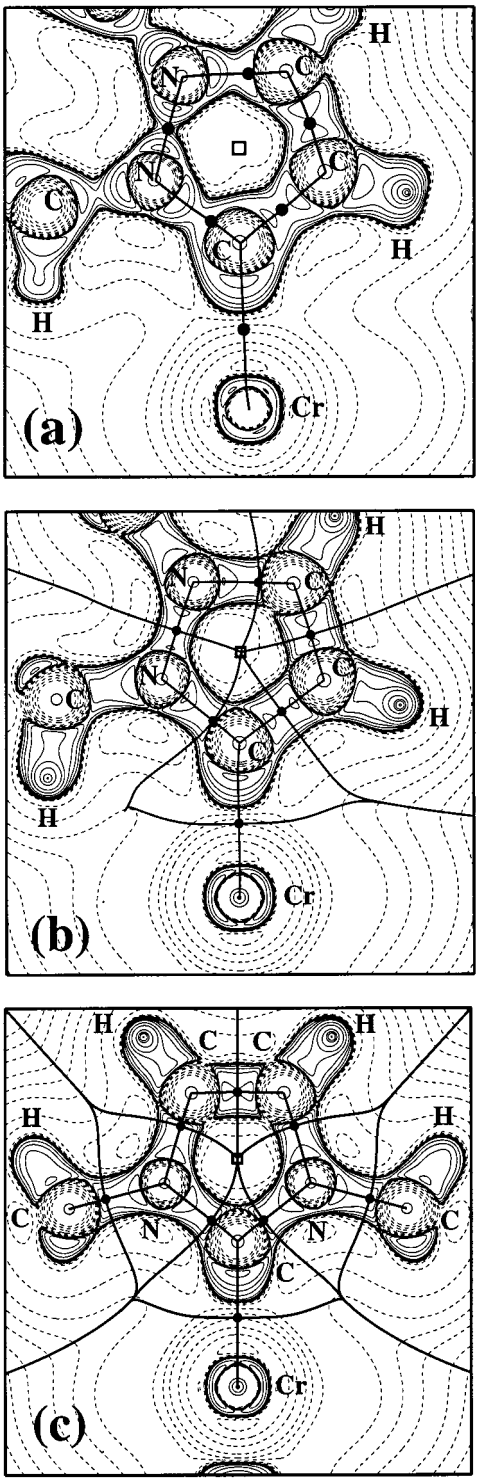

Figure 3. Contour maps of the Laplacian of the experimental (a), and theoretical (BPW91/I) (b) electron density for **1**, and theoretical electron density (BPW91/I) for **2** (c), projected onto the $N-C_{carb}-X$ (X = C for **1** and X = N for **2**) plane of the *N*-heterocyclic five-membered ring. Contour levels are drawn at 0.000, $\pm2.0 \times 10^n$, $\pm4.0 \times 10^n$, $\pm8.0 \times 10^n$ e Å^{-5}, where $n = 0, -3, \pm2, \pm1$; positive and negative values are marked by dashed and solid lines, respectively. The BCPs are denoted by closed circles; ring critical points (RCPs) are marked by open squares; calculated atomic boundaries, as determined by the zero-flux surface condition, along with the bond paths established in the experimental and theoretical electron densities are shown by solid lines.

of **1a** and **2a** as ligands. The locations of the three BCPs – which limit the expansion of the atomic basin of the carbene C

(24) Because of the availability of high-resolution data for **1**, even subtle differences in the axial and equatorial Cr−CO bond lengths of 1.8557(4) and 1.8816(4)−1.9104(4) Å, respectively, can be revealed. Thus, the average Cr−CO bond distances in **1** of 1.8888(2) Å are somewhat shorter than those in $Cr(CO)_6$ [$Cr-CO_{av} = 1.915(4)$ Å]; see ref 25, where six, rather than five, strong π-acceptor CO ligands compete for electron density at the Cr atom. This confirms that *N*-heterocyclic carbene **1a** is a significantly weaker π-acceptor ligand than CO; see ref 26. Furthermore, the C−O bond lengths of 1.159(1) Å (axial) and 1.148 Å (equatorial, averaged) in **1** can be resolved [$C-O_{av} = 1.140$ Å in $Cr(CO)_6$; see ref 25], in good agreement with the classical bonding model in metal carbonyls [see, for example: Fischer, H.; Kreissl, F. R.; Schubert, U.; Hofmann, P.; Dötz, K. H.; Weiss, K. *Transition Metal Carbene Complexes*; VCH Publishers: Weinheim, Germany, 1984.] These trends are also supported by theory; calculated Cr−CO bond distances are 1.868 Å (axial) and 1.891 Å (equatorial) in **1**, and 1.906 Å in $Cr(CO)_6$. We note that the calculated C−O bond length, 1.178 Å, is significantly overestimated at the BPW91/I level of theory as compared with the averaged experimental value (1.1505(3) Å).

(25) Rees B.; Mitschler, A. *J. Am. Chem. Soc.* **1976**, *98*, 7918−7924.

(26) A proper comparison of experimental structural parameters (especially bond distances) should be based on low-temperature high-resolution X-ray or neutron diffraction data ($d < 0.5$ Å) which minimize systematic errors in bond distances. Typically, low-resolution X-ray structures tend to give artificially short bond lengths owing to difficulties in distinguishing between vibrational effects (both harmonic and anharmonic), and a redistribution of the electron charge density due to bond formation (see, for example, ref 27). Unfortunately, the lack of high-resolution experimental data for most of the systems studied has forced us to base our comparison on the results of the DFT calculations.

(27) Coppens, P. *X-ray Charge Densities and Chemical Bonding*, IUCr Texts on Crystallography; Oxford University Press: Oxford, 1997.

(28) Tsirelson, V. G.; Ozerov, R. P. *Electron Density and Bonding in Crystals*; Institute of Physics Publishing: Bristol, 1996.

(29) (a) Koritsanszky, T. S.; Coppens, P. *Chem. Rev.* **2001**, *101*, 1583−1628. (b) Popelier, P. L. A.; Aicken, F.; O'Brien, S. E. In *Chemical Modelling: Applications and Theory*; Hinchliffe, A., Ed.; Royal Society of Chemistry Specialist Periodical Report, 2000; Chapter 3, Vol. 1, pp 143−198.

(30) (a) Cremer, D.; Kraka, E. *Croat. Chem. Acta* **1984**, *56*, 1259−1281. (b) Cremer, D.; Kraka, E. *Angew. Chem.* **1984**, *96*, 612−613; *Angew. Chem., Int. Ed. Engl.* **1984**, *23*, 627−628.

(31) The ratios $G(\mathbf{r}_c)/\rho(\mathbf{r}_c) < 1$, and $H(\mathbf{r}c) < 0$, both characterize a shared interaction (covalent bonds), while for a closed-shell (or unshared) interaction (ionic, hydrogen, or van der Waal's bonds), the value of $G(\mathbf{r}_c)/\rho(\mathbf{r}_c) > 1$ is found; see refs 13 and 30.

(32) This effect is most significant for polar multiple bonds and might indicate an insufficient level of theory. Thus, the Laplacian of the charge density may prove a very sensitive criterion to detect insufficient description of electronic structures.

(33) The definition and classification of the chemical bond in the topological analysis are based on (a) the existence of a BCP in the total electron density, $\rho(\mathbf{r}_c)$, between neighboring atoms, and (b) on a bond path which follows the maximum electron density and terminates at the neighboring nuclei in the equilibrium state. The presence of a bond path is the necessary and sufficient condition for bonding between the two nuclei in the theory of atoms in molecules; see ref 34. The set of all bond paths in a molecule provides a topological definition of molecular structure by indicating the dominant interactions between atoms; see ref 34.

(34) Bader, R. F. W. *J. Phys. Chem.* **1998**, *A102*, 7314−7323.

(35) An atomic basin is defined as a region of space bounded by a surface through which the flux in the gradient vector field of the electron density is zero; see ref 13.

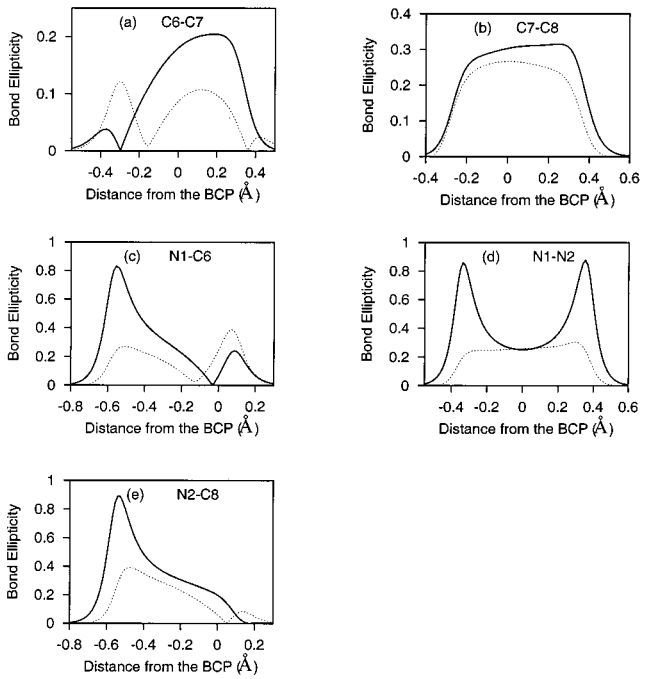

Figure 4. (a−e) Variation in the calculated (solid line) and experimental (broken line) bond ellipticities, ϵ, along the bond paths in the heterocyclic ring in **1** (the numbering of atoms is the same as in Figure 1). Calculated values at the BPW91/I level of theory. For a definition of ϵ, see Figure 5b.

atom in **1** − are rather different;[36] the BCP for the C_{carb}−C lies almost at the midpoint [$d_1(C_{carb}\cdots BCP) = 0.682$ Å; $d_2(BCP\cdots C) = 0.738$ Å; $d(C_{carb}\cdots C) = 1.420$ Å; $r(C_{carb}-C) = 1.420$ Å] (where r and d represent the internuclear distance and bond path, respectively; $d = d_1 + d_2$). In the case of the C_{carb}−N bond, the higher electronegativity of the N atom forces the BCP closer to the C atom [$d_1(C_{carb}\cdots BCP) = 0.473$ Å; $d_2(BCP\cdots N) = 0.884$ Å; $d(C_{carb}\cdots N) = 1.357$ Å; $r(C_{carb}-N) = 1.357$ Å], enlarging the atomic basin of the N atom at the expense of the carbene C atom. The nearly identical distances and path lengths for the C_{carb}−N and C_{carb}−C bonds show them to be linear and reveal no evidence of ring strain.

Analysis of the Bond Path. The π-character of a bond may be revealed by the bond ellipticity ϵ, which measures the asymmetry of the charge distribution between two bonded atoms. While for nonpolar bonds ϵ provides a rather sensitive measure of the degree of π-delocalization, the interpretation becomes more difficult in the case of heteropolar bonds such as C−N.[37] Here, the value of ϵ at the BCP *alone* is not indicative of the preferred plane of polarization (major axis) of the valence electron density. In extreme cases, the BCPs of polar bonds are shifted significantly toward the more electropositive atom. In this case, polarization effects caused by valence shell charge concentrations (VSCCs) can dominate the direction of the major axis. Cheeseman et al.[37] thus examined preferentially the *profile* of ϵ along the bond path between the bonded atoms. Figure 4 traces the bond paths within the heterocyclic ring of **1** derived by experiment and theory.[38] The topological analysis of the BPW91/I electron density reproduces qualitatively all the main features found in the experimental bond ellipticities, but quantitative agreement is poor. In the following discussion, we refer to the calculated values as a common basis for comparing topological features of **1** with the model compounds.

Analysis of the theoretical and experimental data shows all bond paths in the heterocycle to have characteristic profiles, with $\epsilon > 0$ at the BCPs. However, for purely delocalized systems, the major axes of ϵ should always be oriented *perpendicular* to the ring plane along the complete bond paths;[38] this is not the case for the C_{carb}−N bond, even at the BCP. In contrast, the C_{carb}−C_{sp^2} bond displays a perpendicular alignment of the major axis along with a pronounced ellipticity at the BCP (Table 3), in accord with the experimental data. For **2a**, a similar situation is observed; again, the cyclic electronic delocalization seems to be hindered by the presence of the carbene C atom. However, in contrast to **1** and the free carbene **2a**, significant ellipticity and a perpendicularly oriented major axis are observed at the BCP, suggesting slightly greater cyclic π-delocalization in **2** versus **2a** and **1** (Figure 5a).

This situation changes dramatically when the imidazolium cation **2b** is considered. Figure 5a shows the variation in ϵ along the C−N bond path for a number of species calculated at the *same* level of theory (BPW91/I). These data provide an extremely sensitive measure of changes in the heterocyclic ring on going from the free carbene **2a** to the complex **2**. From these profiles, we conclude that the ellipticity of the C−N bonds in the carbene ligand in **2** resembles that in the free carbene **2a** more closely than that in the imidazolium cation **2b**. At the same time, the electron density in the carbene ligand of complex **2** is more cyclic delocalized, as revealed by the larger range of the perpendicularly oriented major axis with respect to the ring plane than that for the free carbene **2a** ($-0.1 < d < 0.9$ in **2** vs $0.02 < d < 0.9$ in **2a**; d is the distance from BCP; see Figure 5a).[39]

Table 3 lists local topological parameters at the BCP in the theoretical electron density for all bonds in the five-membered rings of complexes **1** and **2**, carbenes **1a** and **2a**, and their protonated analogues **1b** and **2b**.

To study the sensitivity of the topological parameters at the level of theory employed, we selected the free carbene **2a** and performed a topological analysis of the theoretical charge densities based on Hartree−Fock and DFT calculations using basis sets of different size and quality.

The results are summarized in Table 4 and confirm for cyclic carbenes the general trend of decreasing electron density at the BCPs when electron correlation is taken into account.[40,41] In

(36) It has been shown (see ref 13) that in the heteronuclear C−N and C−O bonds, the BCP lies significantly closer to the less electronegative C atom, indicating a greater accumulation of electron charge density closer to the more electronegative N or O atom. In the homonuclear C−C bonds, the BCP is centered approximately between the two C atoms.

(37) Cheeseman, J. R.; Carroll, M. T.; Bader, R. F. W. *Chem. Phys. Lett.* **1988**, *143*, 450−458.

(38) Profiles presented in Figure 4 are qualitatively similar as compared with the one shown in Figure 2c of ref 37 for the C−N bond path in the formamide monomer; each curve shows two maxima and one minimum with the latter being in the vicinity of the BCP.

(39) A similar study based on theoretical calculations for *N*-heterocyclic carbene, silylene, and germylene complexes of M−Cl (M = Cu, Ag, Au) has been performed by Frenking et al. (see ref 22e). Our study together with the previous one (see ref 22e) agree on the fact that the electron delocalization in the cyclic carbenes are enhanced by coordination to metal carbonyls.

(40) Wiberg, K. B.; Hadad, C. M.; LePage, T. J.; Breneman, C. M.; Frisch, M. J. *J. Phys. Chem.* **1992**, *96*, 671−679.

(41) Inclusion of electron correlation changes the charge-density distribution dramatically. Møller−Plesset perturbation theory calculations (MP2), configuration interaction with single and double excitations (CISD), and quadratic CI (QCI) showed that the main effect of correlation is to *reduce* the charge density at the BCP; that is, charge is depleted in the bonding regions for correlated densities with respect to the HF method. At the same time, an increase is observed in charge density in shells around the atomic nuclei and at the periphery of the molecule (see ref 42).

Table 3. Theoretical Topological Parameters for **1**, **2**, **1a**, **2a**, and the Protonated Species **1b** and **2b**[a]

bond	r_e(A–B), [Å]	$\rho(\mathbf{r}_c)$, [e Å^{-3}]	$\nabla^2\rho(\mathbf{r}_c)$, [e Å^{-5}]	ϵ^b	bond	r_e(A–B), [Å]	$\rho(\mathbf{r}_c)$, [e Å^{-3}]	$\nabla^2\rho(\mathbf{r}_c)$, [e Å^{-5}]	ϵ^b
1a					**2a**				
$C_{carb}-N$	1.355	1.94	−4.1	0.35 (||)	$C_{carb}-N$	1.382	1.93	−12.9	0.03 (||)
N−N	1.423	2.04	−10.5	0.23 (⊥)	N−C	1.397	1.93	−15.5	0.21 (⊥)
N−C	1.368	2.00	−13.6	0.19 (⊥)	C═C	1.372	2.12	−19.8	0.41 (⊥)
C═C	1.390	2.02	−18.2	0.30 (⊥)	**2**				
$C_{carb}-C$	1.444	1.87	−16.5	0.10 (⊥)	$C_{carb}-N$	1.383	1.97	−15.2	0.13 (⊥)
1					N−C	1.392	1.95	−15.5	0.21 (⊥)
$C_{carb}-N$	1.374	1.91	−9.1	0.06 (||)	C═C	1.366	2.14	−20.3	0.40 (⊥)
N−N	1.395	2.19	−13.7	0.25 (⊥)	**2b**				
N−C	1.362	2.02	−12.7	0.20 (⊥)	C−N	1.350	2.14	−17.6	0.34 (⊥)
C═C	1.387	2.05	−18.8	0.30 (⊥)	N−C	1.389	1.93	−13.9	0.20 (⊥)
$C_{carb}-C$	1.432	1.92	−17.2	0.18 (⊥)	C═C	1.376	2.12	−19.9	0.39 (⊥)
1b									
C−N	1.358	2.03	−11.8	0.20 (⊥)					
N−N	1.373	2.31	−15.8	0.26 (⊥)					
C═C	1.399	2.02	−18.5	0.27 (⊥)					

[a] BPW91/I level. [b] Direction of the major axis with respect to the heterocyclic ring plane at the bond critical point in parentheses.

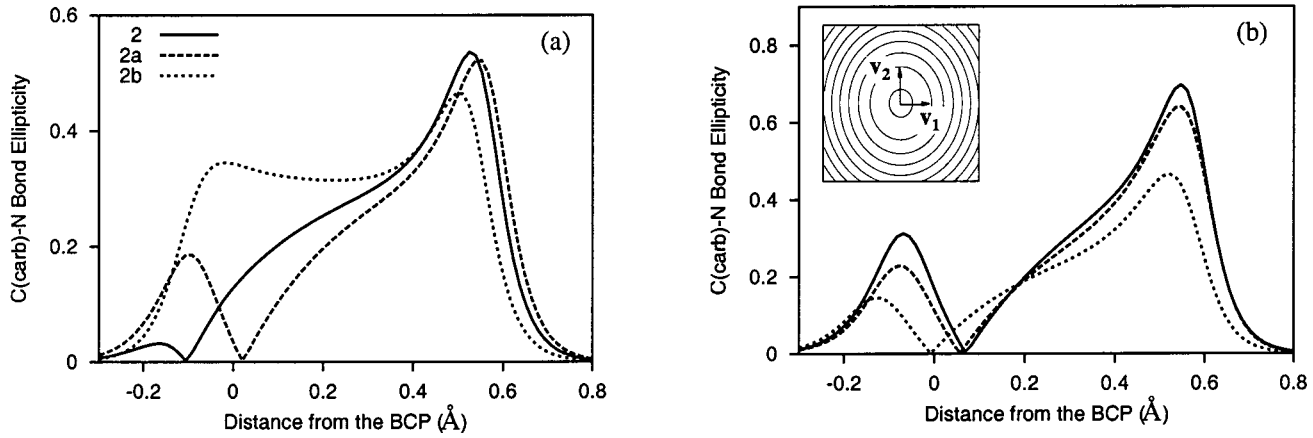

Figure 5. (a) The variation in ϵ along the $C_{carb}-N$ bond path in **2**, **2a**, and **2b** calculated at the BPW91/I level of theory. (b) Values of ϵ in **2a** along the $C_{carb}-N$ bond path at various level of theory: HF/I (solid), HF/6-311++G(3df,3pd) (long-dashed), BPW91/6-311++G(3df,3pd) (short-dashed). The BCP is at the origin of each plot. The left-hand nucleus is the carbene C atom. The definition of ϵ is illustrated by the $\rho(\mathbf{r})$ contour map in the inset of (b) showing the calculated charge density (BPW91/I) in the plane perpendicular to the bond path at the C═C BCP of **2a**. ϵ is thus a measure of the nonspherical charge distribution of $\rho(\mathbf{r})$; $\mathbf{v}_1$ and $\mathbf{v}_2$ are two eigenvectors perpendicular to the C═C bond path at the BCP with the corresponding *negative* eigenvalues λ_1 (minor axis) and λ_2 (major axis) of the Hessian matrix of $\rho(\mathbf{r})$ with $|\lambda_2| < |\lambda_1|$ and $\epsilon = \lambda_1/\lambda_2 - 1$.

Table 4. Theoretical Topological Parameters for the Free Carbene **2a**[a]

bond	HF/I	HF/6-311++G(3df,3pd)	BPW91/I	BPW91/6-311++G(3df,3pd)	MP2(FC)/I
$C_{carb}-N$					
r_e(A−B)	1.3509	1.3451	1.3821	1.3719	1.3810
$\rho(\mathbf{r}_c)$	2.10	2.22	1.93	2.07	1.92
$\nabla^2\rho(\mathbf{r}_c)$	−11.71	−15.88	−12.92	−18.91	−11.76
ϵ^b	0.17 (||)	0.11 (||)	0.03 (||)	0.01 (⊥)	0.01 (||)
N−C					
r_e(A−B)	1.3843	1.3802	1.3971	1.3905	1.3871
$\rho(\mathbf{r}_c)$	2.03	2.13	1.93	2.03	1.96
$\nabla^2\rho(\mathbf{r}_c)$	−18.47	−21.19	−15.47	−19.59	−16.07
ϵ^b	0.16 (⊥)	0.14 (⊥)	0.21 (⊥)	0.19 (⊥)	0.23 (⊥)
C═C					
r_e(A−B)	1.3367	1.3307	1.3721	1.3614	1.3790
$\rho(\mathbf{r}_c)$	2.34	2.48	2.12	2.23	2.10
$\nabla^2\rho(\mathbf{r}_c)$	−25.44	−30.18	−19.85	−22.74	−19.76
ϵ^b	0.52 (⊥)	0.45 (⊥)	0.41 (⊥)	0.34 (⊥)	0.41 (⊥)

[a] r_e in Å, $\rho(\mathbf{r}_c)$ in e Å^{-3}, $\nabla^2\rho(\mathbf{r}_c)$ in e Å^{-5}. [b] Direction of the major axis with respect to the molecular plane at the bond critical point in parentheses.

addition, the dependence of the AIM analysis on the basis set is revealed.[42] Particularly for the $C_{carb}-N$ bond, inclusion of electron correlation leads to a significant decrease not only in the electron density at the BCPs,[43] but also in ϵ. Furthermore, use of a larger basis set causes the minimum value of ϵ to approach the BCP such that, at the BPW91/6-311++G(3df,-3pd) level, the $C_{carb}-N$ BCP in **2a** appears in the region where the major axis is perpendicular to the ring plane (see also Figure 5b).[44] However, in contrast to **2a**, the $C_{carb}-N$ BCP in **1a** still

(42) (a) Wang, J.; Eriksson, L. A.; Johnson, B. G.; Boyd, R. J. *J. Phys. Chem.* **1996**, *100*, 5274−5280. (b) Wang, J.; Eriksson, L. A.; Boyd, R. J.; Shi, Z.; Johnson, B. G. *J. Phys. Chem.* **1994**, *98*, 1844−1850.

(43) Gatti, C.; MacDougall, P. J.; Bader, R. F. W. *J. Chem. Phys.* **1988**, *88*, 3792−3804 and references therein.

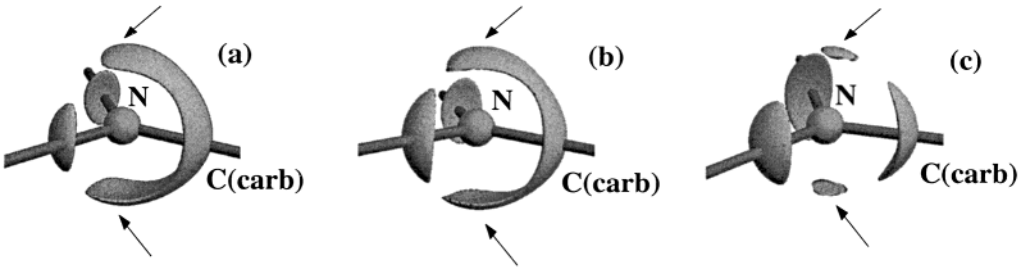

Figure 6. Isosurface map of the Laplacian of the theoretical (BPW91/I) charge density ($\nabla^2\rho(\mathbf{r}) = -32.5$ e Å^{-5}) of **2a** (a), **2** (b), and **2b** (c) showing charge concentrations (CCs) located at the N atom above and below the heterocyclic ring plane (indicated by arrows). The CCs are more pronounced in **2** and **2a** than in **2b**, indicating less effective cyclic π electron delocalization in **2** and **2a**.

lies close to the carbene C atom where the major axis is *in* the plane of the ring, but also in close proximity to the minimum value of ϵ. This signals a lower degree of cyclic π-electron delocalization of the $C_{carb}-N$ bond in **1a** versus **2a**. In contrast to standard theoretical criteria such as analysis of the p_π occupancy at the carbene center, this method allows us not only to distinguish between the electronic structure of carbenes **1a** and **2a**, but reveals more subtle differences in the π-electron delocalization of the individual bonds. Furthermore, analysis of the complete bond paths provides a more robust, less method-dependent criterion than does a simple analysis of topological features at the BCPs.[11f]

2.4. Laplacian of the Charge Density. Localization of Lone Pairs in the Laplacian. The Laplacian of the electron density, $\nabla^2\rho(\mathbf{r})$, has been definitively shown to reveal local charge concentrations (CC) and local charge depletions (CD) in the electron distribution, highlighting subtleties in the bonding of main-group compounds as well as transition-metal complexes.[13] Bader et al.[45] state that "the Laplacian distribution provides a bridge between the density and orbital approaches to the understanding of chemical reactivity".[46] In addition, the Laplacian can be reliably used to predict reactive sites, such as the positions of electrophilic attack in aromatic systems,[47] or the preferred site of protonation of a molecule. Charge concentrations can thus serve as an analogue of the localized lone pairs in the Lewis model.[48]

In Figure 6a, the isosurface map of the Laplacian [$\nabla^2\rho(\mathbf{r}) = -32.5$ e Å^{-5}] for **2a**, **2**, and **2b** reveals localized CCs at the N atoms above the heterocyclic ring plane. In the imidazolium cation **2b**, these nearly vanish (Figure 6c), consonant with a delocalized π-electron system. However, as already indicated by the ellipticity profiles, **2a** and **2** show large CCs at the N atoms, characteristic of hindered π-electron delocalization. In **2a**, the nonbonded CCs at the N atoms merge with the bonded CC of the N−C(carbene) bond to form a broad feature, while in **2** increased π-delocalization results in a narrowing of this feature (see arrows in Figure 6b).[49] In agreement with the results

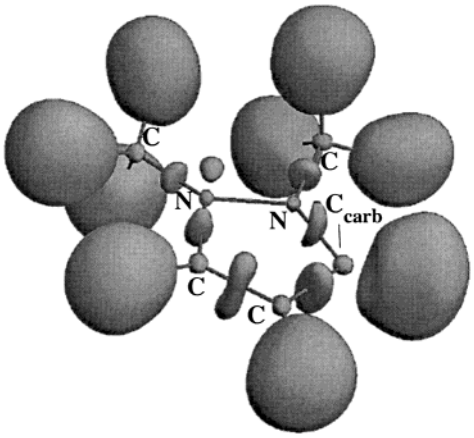

Figure 7. Isosurface plot of the ELF (0.87) of the ring plane in **1a** showing the significant degree of π-delocalization along the $C_{carb}-C_{sp^2}$ bond in comparison with the $C_{carb}-N$ bond.

of the bond-path analysis, the electron delocalization along the $C_{carb}-C_{sp^2}$ bond in **1** appears less hindered than that along the more polar $C_{carb}-N$ bond. This conclusion is supported by the electron localization function (ELF)[50] for **1a**, as shown in Figure 7. This plot (ELF = 0.87) clearly indicates (i) partial delocalization of the lone pair domain at the N atom adjacent to the carbene C atom, (ii) a higher degree of electron localization at the second N atom, which projects a lone pair above the ring plane, and (iii) the typical π-type shape of the ELF domain elongated perpendicular to the $C_{carb}-C_{sp^2}$ bond. Thus, for both

(44) In a previous study by Heinemann et al. (see ref 11f), the topological parameters for a number of carbene model systems were calculated at the HF/6-31G(d) level of theory. According to our findings, HF wave functions may be inadequate to describing the topology of the charge density in cyclic aminocarbenes.

(45) Bader, R. F. W.; MacDougall, P. J. *J. Am. Chem. Soc*. **1985**, *107*, 6788−6795.

(46) Popelier, P. L. A. *Coord. Chem. Rev*. **2000**, *197*, 169−189 and references therein.

(47) Bader, R. F. W.; Chang, C. *J. Phys. Chem*. **1989**, *93*, 2946−2956.

(48) (a) Gillespie, R. J.; Robinson, E. A. *Angew. Chem.* **1996**, *108*, 539−560; *Angew. Chem., Int. Ed. Engl.* **1996**, *35*, 495−514. (b) Gillespie, R. J.; Bytheway, I.; Tang, T.-H.; Bader, R. F. W. *Inorg. Chem*. **1996**, *35*, 3954−3963. (c) Bader, R. F. W.; Gillespie, R. J.; Martîn, F. *Chem. Phys. Lett.* **1998**, *290*, 488−494.

(49) We note that the broad feature of the bonded and nonbonded CCs in **2** and **2a** causes numerical difficulties in locating the exact positions of the CCs, possibly explaining inconsistencies in the numbers of CCs found at N by different numerical methods (as implemented in programs available to us). These methods might even fail to locate CCs when the Laplacian of the charge density is as diffuse as in **2a** and **2** − thus, graphical inspection by isosurface plots is more reliable. The quality of the wave function itself is also of importance; see ref 11f.

(50) The electron localization function (ELF) introduced by Becke and Edgecombe [Becke, A. D.; Edgecombe, K. E. *J. Chem. Phys*. **1990**, *92*, 5397−5403] has been successfully used to reveal the atomic shell structure, chemical bonds, and nonbonding charge concentrations (lone pairs) in various chemical systems both in the gas phase and in solids [(a) Silvi, B.; Savin, A. *Nature* **1994**, *371*, 683−686. (b) Savin, A.; Nesper, R.; Wengert, S.; Fässler, T. F. *Angew. Chem.* **1997**, *109*, 1892−1918; *Angew. Chem., Int. Ed. Engl.* **1997**, *36*, 1808−1832]. The ELF is a quantum mechanical quantity which is shown to be closely related to the Pauli exclusion principle [Savin, A.; Jepsen, O.; Flad, J.; Andersen, O. K.; Preuss, H.; von Schnering, H. G. *Angew. Chem.* **1992**, *104*, 186−187; *Angew. Chem., Int. Ed. Engl.* **1992**, *31*, 187−188]. The ELF is based on a measurable property of a system, viz., the total electron density, and thus has an advantage over the localized molecular orbital formalism. This function, defined so as to be in the range of values $0 \le \mathrm{ELF} \le 1$, makes it possible to reveal the regions of the local electron localization, where ELF ≈ 1. Moreover, a topological analysis of the ELF based on its gradient field has led to a deeper understanding of the chemical bonding in various systems studied to date. Such an analysis can be complementary or sometimes even superior to that based on the analysis of the Laplacian of the electron density [Bader, R. F. W.; Johnson, S.; Tang, T.-H.; Popelier, P. L. A. *J. Phys. Chem*. **1996**, *100*, 15398−15415].

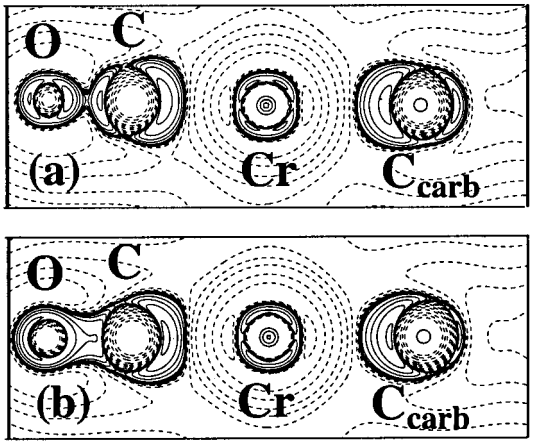

Figure 8. Contour maps of the Laplacian of the experimental (a) and theoretical (BPW91/I) (b) electron density for **1** projected onto the plane perpendicular to the N−C_{carb}−C plane and containing the Cr−C_{carb} bond. Contour levels are the same as in Figure 3.

1a and **1**, the extent of π-donation ($R_2N-C-R \leftrightarrow R_2N^+=C^--R$) is small, and the carbene center is well integrated in a delocalized π-system only from one side via the $C_{carb}-C_{sp^2}$ bond. Hence, the stabilization of *N*-heterocyclic carbenes seems to arise primarily from the enhanced $-I$ effect of the N atoms. Our results are consonant with the conclusion reached by Arduengo that the lone pairs of the N atoms are indeed localized, and might contribute to the kinetic stability observed for the free *N*-heterocyclic carbene species.[5]

Experimental Prediction of Reactive Sites (Centers of Local Lewis Basicity/Acidity). Recently, Frenking et al. showed that the Laplacian of the theoretical charge density can be used to distinguish between the nature and reactivity of Fischer- and Schrock-type carbenes.[22d] We have attempted to use this criterion to classify a series of related carbene complexes. Figure 3 shows the Laplacian of the experimental and theoretical (BPW91/I) electron densities projected onto the plane of the *N*-heterocyclic five-membered ring of **1**, while in Figure 8 the Laplacian perpendicular to this plane − containing the Cr−C_{carb} bond − is depicted. There is good agreement between the theoretical and the experimental Laplacian distribution in both planes of projection. Furthermore, the distribution in the p_π plane of the carbene center (perpendicular to the ring plane) reveals centers of local Lewis acidity and basicity. Figure 9a and b shows the calculated Laplacian distribution around the carbene C atom for the two Fischer-type model systems **6** and **7**, respectively, for the heterocyclic complexes **8** (Figure 9c) and **2** (Figure 9d), and for the free carbene **2a** (Figure 9e). The carbene C atom in the Fischer complexes **6** and **7** clearly exhibits a region of *local charge depletion* in the p_π plane, as indicated by arrows in Figure 9a and b.[51] These regions of charge depletion and concomitant local Lewis acidity may represent favored positions for nucleophilic attack as proposed by Frenking et al.[22d] In contrast to the Fischer complexes **6** and **7**, the carbene centers in both **1** and **2** are shielded by unbroken regions of *local charge concentration* (Figures 8 and 9d). In addition, Figure 9c clearly shows the Laplacian distribution at the carbene center of saturated Arduengo carbene **8** to resemble

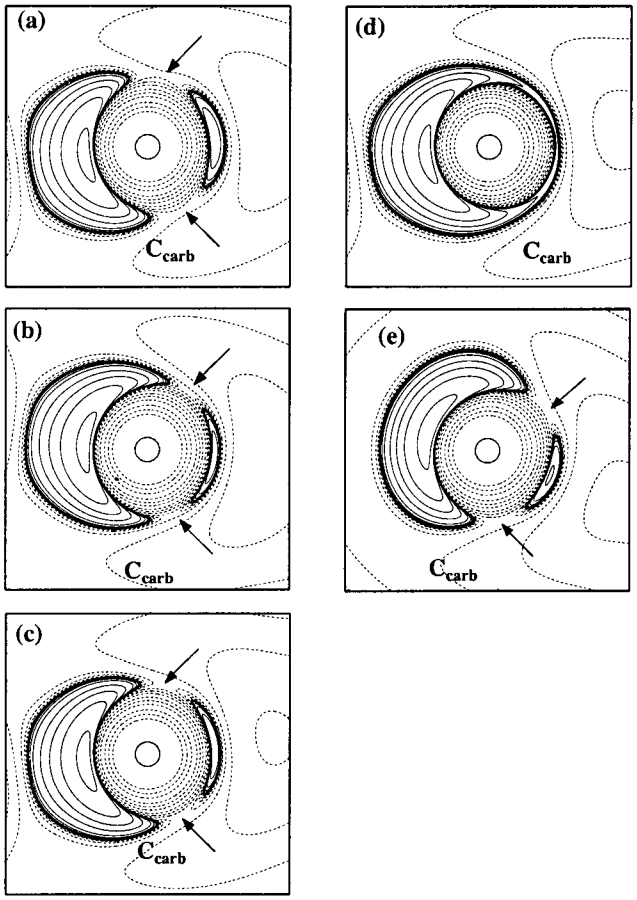

Figure 9. Contour maps of the Laplacian of the theoretical electron density (BPW91/I) for **6** (a), **7** (b), **8** (c), **2** (d), and **2a** (e) in the plane perpendicular to the N−C_{carb}−X plane (X = N or C) and containing the Cr−C_{carb} bond or bisecting the N−C_{carb}−N angle for **2a**. Contour levels are the same as in Figure 3.

those calculated for the noncyclic Fischer carbenes **6** and **7**, and for the free carbene **2a** (Figure 9e). Hence, the Laplacian distribution shows that the presence of a C=C bond in the *N*-heterocyclic carbene ligands in **1** and **2** has indeed some influence on the chemical reactivity of the carbene center and on the stability of the carbene.

Polarization of the Metal Centers in Carbene Complexes. Analysis of valence-shell charge concentrations [CCs, or local maxima in $-\nabla^2\rho(\mathbf{r})$], and charge depletions [CDs, or local minima in $-\nabla^2\rho(\mathbf{r})$], in the electron density provide a physical basis for the valence shell electron pair repulsion (VSEPR) model.[52] This model rationalizes successfully even the geometries displayed by many transition-metal complexes.[48,53] The negative Laplacian, $-\nabla^2\rho(\mathbf{r})$, of the experimental and theoretical charge-density distribution in **1** and **2** reveals in each case a significantly polarized core for the Cr atom (Figure 10). Six local CDs are found in an octahedral arrangement around the Cr atom such that each points to a corresponding local CC of the ligands (Figure 10b), whereas eight local CCs are found on the faces of this octahedron (Figure 10a).[48] Table 5 compares the properties of the various critical points in the negative

(51) A similar pattern of charge depletion about the carbene center was observed by Wang et al. (see ref 15) in an experimental and theoretical charge-density study on the $(CO)_5Cr=C(OMe)C\equiv CPh$ (see Figure 6e and f there), but was not commented upon.

(52) (a) Gillespie, R. J. *Molecular Geometry*; Van Nostrand Reinhold: London, 1972. (b) Gillespie, R. J.; Hargittai, I. *The VSEPR Model of Molecular Geometry*; Allyn and Bacon: Needham Heights, MA, 1991. (c) Kaupp, M. *Angew. Chem.* **2001**, *113*, 3642−3677; *Angew. Chem., Int. Ed.* **2001**, *40*, 3534−3565.

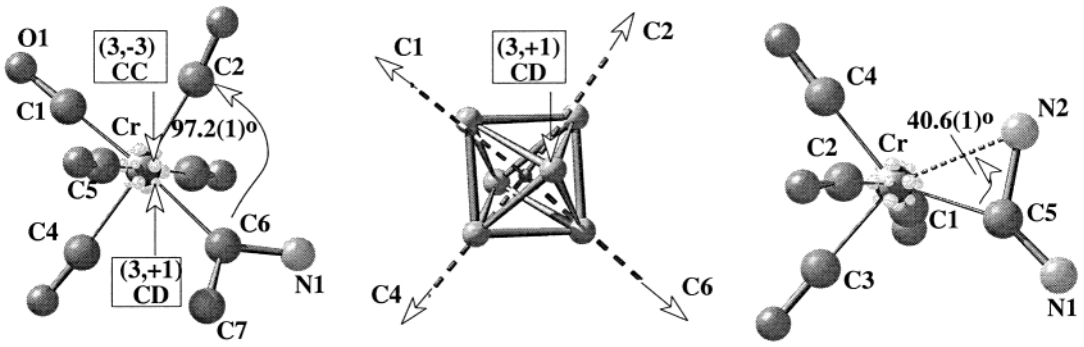

Figure 10. Comparison of the polarization of the metal centers in the hexa-coordinated metal complexes **1** and **10**. (a) Six local CDs (small spheres) as located by (3,+1) CPs in the negative Laplacian of the experimental charge density [$-\nabla^2\rho(\mathbf{r})$] of **1** are found in an octahedral arrangement around the Cr atom such that each points to corresponding local CCs of the ligand, whereas eight local CCs (large spheres), as revealed by (3,−3) CPs, are found on the faces of this octahedron. (b) Octahedral coordination polyhedron formed by the six CDs of **1**. (c) In **10** the carbene ligand coordinates side-on. Thus, two of the six CDs of the octahedron are "ligated" by two donor atoms of the carbene ligand [$C(5)_{carb}$, N2]. However, due to the small bite angle $\angle C_{carb}CrN2$ of 40.6(1)°, the two ligating atoms (C_{carb} and N) cannot match the CDs on the Cr core exactly, and a distorted octahedral geometry is observed.

Table 5. Atomic Graph of the Cr Atom in **1**: Type, Magnitude, and Distance from the Metal Center of all CPs

type	*n*	*r*, [Å]	$\rho(\mathbf{r}_c)$, [e Å^{-3}]	$-\nabla^2\rho(\mathbf{r}_c)$, [e Å^{-5}]
(3, −3)	8			
exp		0.363	14.9−15.4	464−508
calc		0.352	16.0	556−572
(3, +1)	6			
exp		0.372	12.6−13.1	149−183
calc		0.370	13.0	186−202
(3, −1)	12			
exp		0.365	14.2−14.8	382−426
calc		0.356	15.2	443−474

Laplacian of $\rho(\mathbf{r})$ for the Cr atom. Theory and experiment agree on the shell radius (0.35−0.37 Å) around the metal center where the critical points are found. Theoretical values of the electron density at the critical points also compare well with those observed experimentally (see Table 5). However, the calculated values of $-\nabla^2\rho(\mathbf{r})$ for the (3,−3), (3,−1), and (3,+1) CPs are found to be systematically larger than those observed experimentally. The CDs of the metal and the CCs of the ligand may be considered to represent sites of Lewis acidity and basicity, respectively.[54,55] We are not aware of any other comparison of the location and properties of the critical points in $-\nabla^2\rho(\mathbf{r})$ on the basis of both experimental and theoretical charge-density distributions. Further combined studies are required to explore whether the differences we observe are systematic.

2.5. Atomic Properties. The average net atomic charges were obtained by integration over the basin of each atom in the carbene species.[13] In comparison with the results of the NPA (Table 2), the polarity of C_{carb}−N bonds in **1** (C_{carb} = +0.24; N = −0.73) and **2** (C_{carb} = +0.65; N = −1.10) is much more pronounced in the AIM analysis. The same is true for the free carbenes **1a** (C_{carb} = +0.27; N = −0.77) and **2a** (C_{carb}= +0.66; N = −1.13). Thus, the chemically distinct natures of each atom in the heterocyclic ring in **1** are clearly revealed.

It is also interesting to compare these charges with those calculated within the generalized atomic polar tensor (GAPT) formalism.[56] The following net atomic charges (in *e*) were calculated for **1** (values for the free carbene, **1a**, in parentheses), C_{carb} +0.56 (−0.25), N(−C_{carb}) −0.10 (+0.04), N(−N) −0.44 (−0.44), C(−C_{carb}) −0.36 (−0.19), C(=C) +0.19 (+0.14), and for **2** (**2a**), C_{carb} +0.60 (−0.10), N −0.34 (−0.29), and C(=C) −0.07 (−0.06). Some trends, such as the polarity of the C_{carb}−N bond, are revealed consistently, independent of the method of analysis used; however, there are also some glaring inconsistencies. For example, both the natural population (Table 2) and GAPT analyses place a large negative net charge on the Cr atom (−0.6 and −2.0 *e*, respectively). This is at odds with the AIM results, where integration over the basin of chromium atom gives values of +1.26 and +1.21 *e* for **1** and **2**, respectively, in accord with the experimental findings. Indeed, our best model gives an experimental charge of +1.31(5) *e* for chromium, derived from the monopole parameters, P_v, in **1**.[57] Thus, no consistent interpretation of the electronic structure of our benchmark systems can be derived on the basis of the computed charges.

(53) The distortion of the metal outer core shell produced by the ligands with significant potential for π-type interactions can explain the octahedral molecular geometry found in both **1** and **2** and $Cr(CO)_6$ itself; see: MacDougall, P. J.; Hall, M. B. *Trans. Am. Cryst. Assoc.* **1990**, *26*, 105−123. This situation is quite different from that observed when σ-bonding ligands, such as H, CH_3, or F are attached to a metal atom with formal d^0 electron configuration. Thus, for CrF_6, we find at the BPW91/I level in accord with ref 48b *six* local CCs in the outer shell of the core of the metal atom, each of which faces the local CD of the ligand (F). In contrast, in the distorted trigonal prismatic geometry of $Cr(CH_3)_6$ (C_{3v} symmetry), six *ligand opposed* CCs − situated at opposite sides with respect to the Cr−C bonds − are found in the Cr valence shell at the same level of theory. Indeed, *different* arrangements and numbers of local CCs and CDs in the metal outer core can result in the *same* coordination geometry around the metal center [for example, the octahedral configurations found in **1**, **2**, $Cr(CO)_6$, and CrF_6].

(54) Abramov, Yu. A.; Brammer, L.; Klooster, W. T.; Bullock, R. M. *Inorg. Chem.* **1998**, *37*, 6317−6328.

(55) Using the data presented in Table 5, the following equation is satisfied in accord with a special case of the Poincaré−Hopf relationship [see: Collard, K.; Hall, G. G. *Int. J. Quantum Chem.* **1977**, *12*, 623−637], where n_{-3}, n_{-1}, and n_{+1} correspond to the number of the (3, −3), (3, −1), and (3, +1) critical points, respectively: $n_{-3} - n_{-1} + n_{+1} = 2$ (see: Bader, R. F. W.; Popelier, P. L. A.; Chang, C. *J. Mol. Struct.* **1992**, *255*, 145−171). We further note that the arrangement of the CCs and CDs is similar to that found experimentally for the Mn atom in *cis*-$HMn(CO)_4PPh_3$ (see ref 54).

(56) Cioslowski, J. *J. Am. Chem. Soc.* **1989**, *111*, 8333−8336.

(57) Indeed, it has been shown by Volkov et al. [Volkov, A.; Gatti, C.; Abramov, Yu.; Coppens, P. *Acta Crystallogr.* **2000**, *A56*, 252−258] that net atomic charges derived from the monopole parameters, P_v (see Experimental Section), and those from AIM analysis applied to the experimental or theoretical electron density, can differ significantly and thus are not directly comparable with each other. Moreover, we found, in agreement with their results, that atomic moments are dependent on the multipole model used. Our results turned out to be almost independent of the treatment of the 4s electron on the Cr atom, which is in accord with the earlier results for $Cr(CO)_6$ by Coppens *et al.* (see ref 69). Therefore, the net atomic charge determined experimentally from the monopole population parameter (P_v) is quite ambiguous mainly because of the diffuseness of the 4s distribution.

However, analysis of atomic quadrupole polarizations may provide a more sensitive measure of the charge distribution in molecules than computed atomic charges. Moreover, we note that the *atomic* charges obtained from the AIM theory are only useful quantities when the *atomic* higher multipoles (dipoles, quadrupoles, etc.) do not deviate significantly from zero.[13,37] In particular, for a system with a plane of symmetry it is highly meaningful to study the in-plane and out-of-plane charge accumulation,[11f,58] by analyzing the two eigenvalues of the traceless quadrupole moment tensor: Q_{xx} and Q_{zz} (the *z* axis is perpendicular to the heterocyclic ring plane). The more negative the value of Q_{zz}, the greater the extent to which electronic charge is removed from the plane of the heterocyclic ring (*xy*-plane) and concentrated along the perpendicular axis (*z*) passing through the corresponding atom of the ring.

For the free carbenes **1a** and **2a**, the charge density of the carbene carbon ($Q_{xx} = -1.997$ and $Q_{zz} = -1.006$ au for **1a**; $Q_{xx} = -2.017$ and $Q_{zz} = -1.281$ au for **2a**) is preferentially accumulated in the *xz*-plane with the value of Q_{xx} being more negative (the *x* axis for the carbene C nucleus points to its lone pair), as may be anticipated for singlet carbenes (see, for example, ref 11f. We note that our axis orientation is different from that used by Heinemann et al. in ref 11f). Significant changes in the quadrupolar polarizations of the carbene C atoms are observed on going from the free carbene species to the corresponding pentacarbonyl chromium complexes **1** and **2**. Here the situation at the carbene center is reversed, with the charge density of the carbene carbons now mainly concentrated along the *z* axis, perpendicular to the ring plane, signaling a high degree of π-delocalization ($Q_{xx} = -0.134$ and $Q_{zz} = -2.113$ au for **1**; $Q_{xx} = 0.005$ and $Q_{zz} = -2.250$ au for **2**).[59] Thus, theoretical findings indicate a promulgation of the charge density *out of* the heterocyclic ring plane. This is an important conclusion, for it reveals directly the changes in charge density and delocalization attendant on complexation, and promises a deeper understanding of the role of these carbene ligands in catalysis.

3. The Nature of the C−N Bond in Acyclic Carbenes. The extent of π-delocalization in aminocarbenes has generally been correlated with the barrier to rotation about the $C_{carb}-N$ bond.[60] For example, in bis(diisopropylamino)carbene, **9a**, the rotational barrier was determined experimentally to be 53 kJ mol^{-1}.[60a] Recent calculations on simple models systems such as $(H_2N)_2C$ suggest even higher barriers to rotation (81 kJ mol^{-1}; B3LYP/6-31G(d) with thermal corrections).[60b] However, these barriers cannot be related solely to the loss of π-bonding caused by out-of-plane rotation. Considerable electronic repulsion between the lone pair at the N atom and the σ-lone pair of the C_{carb} atom will significantly oppose rotation when the amino groups in the transition state are oriented such that the lone pair at the N atom and the σ-lone pair of the C_{carb} atom eclipse each other in the N−C−N-plane ("in, in" conformation). This effect is illustrated in Figure 11a; the contour maps of $\nabla^2\rho(\mathbf{r})$ for the free carbene **9a** ("in, in" conformation) projected into the $N-C_{carb}-N$ plane clearly reveal the repulsion between the lone pairs at the N2 and the C_{carb} atoms as signaled by the presence of large, eclipsing CCs at these atoms. Reduction of the charge density of the carbene lone pair, for example, by complexation should reduce the effect of the lone-pair repulsion and therefore also diminish the barrier to rotation. Indeed, complexation of bis-(diisopropylamino)-carbene with a $Cr(CO)_4$ fragment results in the first example of a new class of chelating diaminocarbene complexes, **10** (Figures 11b and 12).[61]

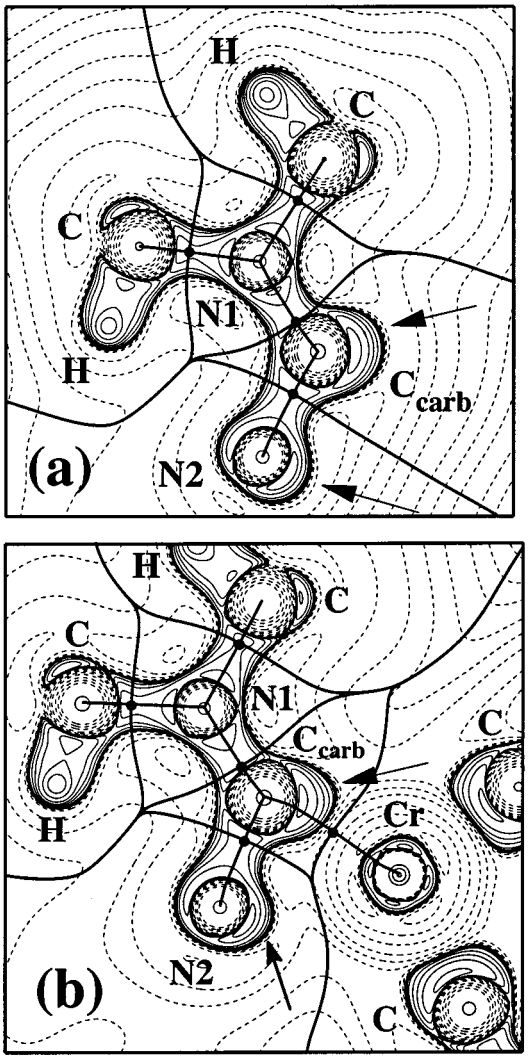

Figure 11. Contour maps of the Laplacian of the theoretical charge density for free carbene **9a** (a) (with one C−N bond displaying an "in, in" conformation), and complex **10** (b) projected onto the $N-C_{carb}-N$ and the $N-Cr-C_{carb}$ plane, respectively (BPW91/I level). Contour levels and symbols used are already specified in Figure 3. The lone pair on the N atom and the C_{carb} atom in **9a** and **10** is indicated by an arrow.

In **10**, the lone pairs at both the metal-coordinating N and the carbene C atoms contribute to donor stabilization of the

(58) Bader, R. F. W.; Chang, C. *J. Phys. Chem.* **1989**, *93*, 2946−2956.
(59) It has been shown by Gatti et al. (see ref 43) that the main effect of electron correlation on the components of atomic quadrupole moments for the *singlet* carbenes is to promote the charge from the *in*-plane orbital (lone pair) into the vacant or partially vacant p_π orbital on the carbene carbon. As a consequence, inclusion of electron correlation causes the values of Q_{zz} to become less positive (or even negative) and the values of Q_{xx} to become less negative as compared to the Hartree−Fock values (see ref 43). Our calculations are in accord with this conclusion; we found that the values of Q_{xx} and Q_{zz} change with the level of theory employed [e.g., Q_{zz} for **2a**: −1.14 au (at HF/I), −1.28 au (at BPW91/I), and −1.46 au (at BPW91/6−311++G(3df, 3pd), and Q_{xx} for **2a**: −2.30 au (at HF/I), −2.02 au (at BPW91/I), and −2.10 au (at BPW91/6−311++G(3df, 3pd)]. Again, these results show atomic quadrupole moments to be sensitive to the level of theory employed, and they should be used with caution, especially as a quantitative probe of the nucleo- or electrophilicity of an atomic site in a molecule.
(60) (a) Alder, R. W.; Allen, P. R.; Murray, M.; Orpen, A. G. *Angew. Chem., Int. Ed. Engl.* **1996**, *35*, 1121−1123. (b) Alder, W. R.; Blake, M. E.; Oliva, J. M. *J. Phys. Chem. A* **1999**, *103*, 11200−11211.

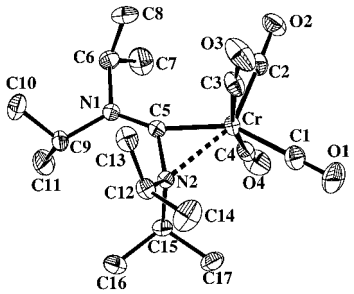

Figure 12. Molecular X-ray structure of **10** at $T = 173$ K: atomic displacement ellipsoids for non-H atoms are drawn at the 50% probability level; hydrogen atoms are omitted for clarity. Selected bond distances [Å] and angles [deg] for **10**: Cr−C1 1.878(2), Cr−C2 1.832(2), Cr−C3 1.879(2), Cr−C4 1.890(2), Cr−C5 1.920(1), Cr···N2 2.207(1), C1−O1 1.157(2), C2−O2 1.166(2), C3−O3 1.151(2), C4−O4 1.151(2), C5−N1 1.309(2), C5−N2 1.457(2), C6−N1 1.491(2), C9−N1 1.502(2), C12−N2 1.533(2), C15−N2 1.507(2), N2−Cr−C5 40.60(5), ∠Cr−N2−C5 59.04(6), ∠Cr−C5−N2 80.36(7).

Lewis-acidic metal center; thus electron density is formally transferred from these donor atoms to the metal, leading to significantly reduced lone-pair repulsion. As shown in Figure 10c, the additional N-donor stabilization is revealed by analysis of the polarization of the metal atom. The negative Laplacian indicates that both donor atoms (N and C_{carb}) face two centers of local CD (centers of increased Lewis acidity) in the outer shell of the core of the Cr atom. This highlights the important contribution made by lone-pair repulsion to the rotational barrier and shows that this barrier cannot be used to measure the extent of π-delocalization.

There is a dramatic shortening of the calculated Cr−C_{carb} bond on chelation (1.914 Å in **10** vs 2.247 Å in **9**) and a significant increase in the charge density and ϵ at the BCP of the Cr−C_{carb} linkage [$\rho(\mathbf{r}) = 0.811$ e Å^{-3}; $\epsilon = 0.31$ for **10** vs $\rho(\mathbf{r}) = 0.43$ e Å^{-3}; $\epsilon = 0.09$ for **9**], signaling a significant degree of double bond character. Inspection of the X-ray structures of complex **10** and free carbene **9a**[9] [(*i*-$Pr_2N)_2C$:] reveals the fundamentally different nature of the C−N bonds in **10**, whereas the C_{carb}−N2 bond in **10** appears significantly elongated [1.457(2) Å in **10** vs 1.363(6)/1.381(6) Å in **9a**]; the pronounced π-character of the C_{carb}−N1 bond is reflected in a rather short bond distance of 1.309(2) Å. Furthermore, both C_{carb}−N bonds in **10** can be distinguished by the relative orientation of their major axes at the corresponding BCPs with respect to the N−C−N plane (C_{carb}−N1, perpendicular; C_{carb}−N2, in-plane). In addition, the major axis of the Cr═C bond has the same (perpendicular) orientation as that displayed by the C_{carb}−N1 bond, suggesting π-electron delocalization within the Cr−C_{carb}−N1 moiety. Thus, the C_{carb}−N1 bond might serve as a benchmark C_{carb}−N bond displaying true π-character.

To date, aminocarbenes have been assumed to be pure σ-donor ligands which can be used in catalysis to complement and extend the capabilities of the ubiquitous phosphane ligands. However, our findings reveal that the coordination chemistry of these systems still leads to surprises which warrant further exploration.

(61) To our knowledge, only a mixed N,P heterocyclic complex displaying a related P-W coordination mode has been described so far; this was interpreted as a potential intermediate in a carbene-carbine rearrangement: Fischer, E. O.; Reitmeier, R. *Angew. Chem.* **1983**, *95*, 419−420; *Angew. Chem., Int. Ed. Engl.* **1983**, *22*, 411−412.

4. Conclusions

This combined experimental and theoretical charge-density study shows that a *direct* analysis of experimental and theoretical electron densities can provide a wealth of information on the nature of chemical bonding in complex systems. Even subtle electronic differences caused by a slight variation in the degree of π-electron delocalization are reliably revealed by a topological analysis of the charge density. We have also shown that the usual analysis of local properties of the electron density alone [such as $\rho(\mathbf{r})$, $\nabla^2\rho(\mathbf{r})$, and ϵ at the BCP] can be misleading in estimating the degree of electron delocalization. Standard criteria of delocalization based on interpretation of the wave function − such as p_π occupations − may also prove misleading, being quite insensitive to changes in the electronic nature of the system as shown for **1a** and **2a**. In such cases, a *full* bond path analysis is found to be more instructive and meaningful. Furthermore, we have demonstrated that topological properties such as bond ellipticities, when evaluated along a full bond path, present a characteristic pattern which is less sensitive to variations in the level of calculations or the choice of experimental multipole model than are topological parameters evaluated at the BCPs alone.

Accordingly, we propose that the following *nonlocal* criteria indicate significant π-electron delocalization in cyclic aminocarbenes: (i) the bond ellipticity, ϵ, along the full bond path deviates significantly from zero, (ii) the orientation of the major axis of ϵ is always perpendicular to the ring plane, (iii) Q_{zz} (a component of the atomic quadrupole moments tensor oriented perpendicular to the ring plane) displays a large negative value; in the case of cyclic carbenes $Q_{zz}/Q_{xx} > 1$ (Q_{xx} is a component of the atomic quadrupole moments tensor oriented along the σ lone pair), and (iv) no significant local charge concentrations exist above and/or below the ring plane at the N atoms to indicate the presence of lone pairs.

On the basis of these criteria, both the pyrazolium **1b** and the imidazolium **2b** cations represent truly delocalized systems, while the charge distribution in the *N*-heterocyclic carbene benchmark systems **1a** and **2a** clearly shows hindered π-electron delocalization. In the corresponding metal complexes **1** and **2**, the degree of electron delocalization is slightly enhanced; however, analysis of the Laplacian of the charge densities still indicates − as in the case of **1a** and **2a** − pronounced local charge concentrations which vitiate complete electron delocalization. In particular, lone pairs are shown to be localized at the N atoms. Indeed, the novel acyclic aminocarbene **10** shows that such lone pairs can even take part in intramolecular coordination to the metal, casting doubts on previous assumptions that large barriers to rotation around the C_{carb}−N bond arise solely from p_π−p_π bonding (R_2N−C:−R ↔ R_2N^+═C^-−R).[60]

5. Experimental Section

Synthesis and Characterization. All reactions and manipulations were carried out under an atmosphere of dry nitrogen using standard Schlenk techniques. Solvents were dried and distilled prior to use. ^{1}H NMR spectra were recorded using a Bruker DPX 400 spectrometer. IR spectra were recorded using a Perkin-Elmer Model 1600 FT-IR spectrometer. Melting points were measured with a Büchi melting point apparatus system (Dr. Tottoli). Elemental analyses were performed at the microanalytical laboratory, Technische Universität München.

Pentacarbonyl-(1,3-dimethylimidazol-2-ylidene)chromium, 2. A solution of 2.05 g (4.77 mmol) of $Na_2Cr_2(CO)_{10}$ in 15 mL of deoxygenated H_2O was added slowly at 0 °C with vigorous stirring to 2.25 g (10.04 mmol) of 1,3-dimethylimidazolium iodide dissolved in z25 mL of deoxygenated H_2O. The resulting yellow microcrystalline precipitate was collected by filtration, washed with 5 × 10 mL of deoxygenated H_2O, and dried in vacuo, to produce bis-(1,3-dimethylimidazolium)decacarbonylochromate(−I). Yield: 2.10 g (78%). This product (3.63 mmol) was heated to 125 °C with stirring in a Schlenk tube attached to a Hg bubbler. The substance melted giving a viscous bubbling liquid. After stirring for 20 min, the Schlenk tube was evacuated and heated for an additional 20 min. On cooling to room temperature, the yellow crystalline mass was dissolved in 25 mL of diethyl ether and separated from the insoluble byproduct tetracarbonyl-bis-(1,3-dimethylimidazol-2-ylidene)chromium by filtration. The filtrate was concentrated in vacuo, and the product was purified by recrystallization from diethyl ether/hexane or by sublimation under high vacuum to give pale yellow crystals. Yield: 1.57 g (78%). Melting point: 100 °C. ^{1}H NMR (400.13 MHz, CD_3CN): δ 3.83 (s, CH_3, 6H), 7.11 (s, C*H*, 2H). IR (hexane, cm^{-1}): ν = 2056 (s, CO), 1925 (vs, CO). Anal. Calcd for $C_{10}H_8CrN_2O_5$: C, 41.68; H, 2.80; N, 9.72. Found: C, 42.33; H, 2.94; N, 9.89.

Pentacarbonyl(1,2-dimethylpyrazol-3-ylidene)chromium, 1. Bis-(1,2-dimethyl-pyrazolium)-decacarbonyldichromate(−I) was prepared in an analogous manner to the procedure above from 2.0 g (4.65 mmol) of $Na_2Cr_2(CO)_{10}$ and 2.2 g (9.82 mmol) of 1,2-dimethylpyrazolium iodide. Next 1.70 g (2.94 mmol) of the product was heated to 150 °C with stirring in a Schlenk tube attached to a Hg bubbler. When the salt was molten the Schlenk tube was evacuated, and heating was continued for 20−30 min until no further gas was evolved. After cooling to room temperature the solidified crystalline brown mass was treated with 5 × 20 mL of diethyl ether, the solution was separated from insoluble dark decomposition products by filtration, and the filtrate was dried in vacuo. The crude crystalline product was dissolved in 20 mL of methanol and filtered through powdered charcoal. This was washed with 5 mL of methanol, and the pale yellow filtrate was concentrated in vacuo to 4−5 mL. After cooling to 0 °C, the mother liquor was removed from the pale yellow crystals by filtration, and the crystals were dried under high vacuum. Evaporation of the mother liquor produced a second crop (8%) of inferior purity. Total yield: 1.0 g (59%). Melting point: 104−106 °C. ^{1}H NMR (400.13 MHz, acetone-d_6): δ 4.11 (s, CH_3, 3H), 4.15 (s, CH_3, 3H), 6.39 (br, C*H*, 1H), 7.73 (br, C*H*, 1H). IR (hexane, cm^{-1}): ν = 2052 (w, CO), 1939 (w, CO), 1927.4 (m, CO), 1919.9 (m, CO). Anal. Calcd for $C_{10}H_8CrN_2O_5$: C, 41.68; H, 2.80; N, 9.72. Found: C, 41.65; H, 2.61; N, 9.65.

Tetracarbonyl{bis(diisopropylamino)carbene}chromium, 10. A solution of 390 mg (1,6 mmol) of $Cr(CO)_6$ in THF was irradiated (Hg immersion lamp; 150 W) at room temperature for 3.5 h with stirring. Next 200 mg (0.94 mmol) of bis(diisopropylamino)carbene, dissolved in 5 mL of THF, was added to the orange solution under vigorous stirring. Stirring for 30 min at room temperature caused the solution to turn reddish brown. The solvent was evaporated in vacuo, and excess $Cr(CO)_6$ was removed by vacuum sublimation. The brown residue was extracted with 3 × 20 mL of diethyl ether. The combined extracts were concentrated to 5 mL in vacuo and separated chromatographically using silica gel/hexane. After elution of a pale yellow zone [mainly $Cr(CO)_6$] with hexane/diethyl ether (2:1), a dark yellow band containing the product was eluted with diethyl ether. The yellow eluate was concentrated to 1−2 mL in vacuo. After adding 5−10 mL of hexane at 0 °C, dark yellow crystals precipitated, which were recrystallized from diethyl ether/hexane. Yield: 80 mg (23%). ^{1}H NMR (400.13 MHz, C_6D_6): δ 0.942 (br, CH_3, 24H), 2.961 (br, C*H*, 4H). IR (hexane, cm^{-1}): ν = 2003.8 (m, CO), 1918.4 (w, CO), 1896.3 (s, CO), 1870.1 (m, CO). Anal. Calcd for $C_{17}H_{28}CrN_2O_4$: C, 54.24; H, 7.50; N, 7.44. Found: C, 54.85; H, 7.39; N, 6.94.

X-ray Data Collection. Crystals of compound **1** were obtained as colorless cubes by slow evaporation of a *n*-hexane solution. A well-faced crystal with dimensions 0.12 × 0.25 × 0.25 mm^3 was glued inside a 0.01 mm thin-walled capillary and mounted on a Nonius kappa-CCD detector system. The sample was cooled with an Oxford Cryostream System to 100.0(1) K with a mean temperature gradient of −2 K/min. Preliminary examination and final data collection were carried out with graphite-monochromated Mo Kα radiation (λ = 0.71073 Å) from a Nonius FR 591 rotating anode running at 50 kV and 80 mA. Intensity data were collected using 1° φ- and ω-scans with a detector-to-sample distance of 40 mm. For the low order data, two φ-scan sets (813 frames in total) at a scan angle (Θ) of 0.0 and 9.8° with a scan time of 8 and 20 s/frame, respectively, and six ω-scan sets (507 frames in total; Θ = −7.3 to −9.8°) with a scan time of 20 s/frame were collected. For the high order data, eight ω-scan sets (813 frames in total; Θ = −17°) with a scan time of 40 s/frame were collected in addition to eight ω-scan sets (1058 frames in total; Θ = −32°) with a scan time of 80 s/frame.[62a] In addition, to test the influence of λ/2 reflections, a φ-scan ($\Delta\varphi$ = 1°, 333 frames) with a scan time of 13.5 s/frame was collected at a lower power (at 50 kV and 40 mA).

X-ray Data Reduction. Crystal data for compound **1** at 100 K: $C_{10}H_8CrN_2O_5$; M_r = 288.18; a = 9.7190(2) Å, b = 6.7650(1) Å, c = 18.1740(4) Å, β = 93.314(1)°, V = 1192.92(4) Å^3; monoclinic; $P2_1/c$; Z = 4; $F(000)$ = 584; D_{calc} = 1.605 g/cm^3; μ = 0.97 mm^{-1}. The unit cell was determined from 10 106 reflection positions. An initial orientation matrix was determined from 10 frames of the first scan set and refined during the integration of the individual scan sets. The intensities were first corrected for beam inhomogeneity and crystal decay by the program SCALEPACK using a tight scale restraint (0.002).[62b] An absorption correction was then applied (T_{min} = 0.840(2), T_{max} = 0.895(2)), and symmetry equivalent and multiply measured reflections were averaged with the SORTAV program,[63] locally modified by one of us (M.T.). The internal agreement factor was $R_{int}(F)$ = 3.8% for a total of 146 231 reflections yielding 12 885 unique reflections. This data set provided 99% of data in 4.2 < 2Θ< 101.6° (sinΘ/λ < 1.09 Å^{-1}).

Determination of Molecular Geometry and Multipolar Refinements. An initial independent atom model (IAM) refinement was carried out, which treated all atoms as spherical. Anisotropic atomic displacement parameters were introduced to describe the thermal motion of all non- hydrogen atoms. All hydrogen atom positions were found in the difference map calculated from the model containing all non-hydrogen atoms. Isotropic temperature parameters for the hydrogen atoms were derived from the parent carbon atom (U_H = 1.5 UC_{sp^3}, U_H = 1.2 UC_{sp^2}). The hydrogen atom positions were then fixed ($r(C_{sp^2}$−H) = 1.08 Å, $r(C_{sp^3}$−H) = 1.09 Å). The refinement finally converged at R_1 = 0.0287, wR_2 = 0.0832, and GOF = 1.34 for 164 parameters with the ratio N_{ref}/N_{var} = 62. The residual electron density map showed the maximum and minimum values of 0.48 and −0.55 e Å^{-3}, respectively.

A multipole model was adopted to describe the deformation of $\rho(\mathbf{r})$ from a spherical distribution. According to a method proposed by Stewart,[64] the electron density $\rho(\mathbf{r})$ in a crystal is described by a sum of aspherical pseudoatoms at the nuclear positions $\{\mathbf{R}_j\}$:

$$\rho(\mathbf{r}) = \sum_j \rho_j(\mathbf{r} - \mathbf{R}_j) \qquad (1)$$

On the basis of the Hansen−Coppens formalism,[65] the pseudoatom density $\rho_j(\mathbf{r} - \mathbf{R}_j)$ is expressed in terms of multipoles ($\mathbf{r}_j = \mathbf{r} - \mathbf{R}_j$):[66b]

(62) (a) "Collect" data collection software; Nonius, B. V., 1998. (b) Otwinowski, Z.; Minor, W. *Processing of X-ray Diffraction Data Collected in Oscillation Mode, Methods in Enzymology*, Volume 276: *Macromolecular Crystallography*, Part A; Carter, C. W., Jr., Sweet, R. M., Eds.; Academic Press: San Diego, CA, 1997; pp 307−326.
(63) Blessing, R. H. *Acta Crystallogr.* **1995**, *A51*, 33−38.
(64) Stewart, R. F. *Acta Crystallogr.* **1976**, *A32*, 565−574.
(65) Hansen, H. K.; Coppens, P. *Acta Crystallogr.* **1978**, *A34*, 909−921.

$$\rho_j(\mathbf{r}_j) = P_c\rho_c(\mathbf{r}_j) + \kappa'^3 P_v\rho_v(\kappa'\mathbf{r}_j) + \sum_{l=0}^{l_{max}} \sum_{m=-l_{max}}^{+l_{max}} \kappa''^3 P_{lm} R_l(\kappa''\mathbf{r}_j) Y_{lm}(\theta_j,\varphi_j) \quad (2)$$

In the refinement of our best model, the multipole expansion was truncated at the hexadecapole level ($l_{max} = 4$) for the Cr, and at the octapole level ($l_{max} = 3$) for the C, N, and O atoms. A bond-directed dipole ($l_{max} = 2$) was also introduced for the hydrogen atoms. Core and spherical valence densities were constructed using Clementi and Roetti Roothaan−Hartree−Fock (RHF)[67] atomic wave functions expanded over Slater-type basis functions (STO); the radial functions for the deformation densities were single-ζ Slater-type orbitals.[68] In our final model, only even order multipoles on the Cr atom were allowed to refine assuming a $3d^5$ valence configuration of chromium while adding the 4s electron to the core.[69] In the refinement, four equatorial CO groups were assumed to be chemically equivalent (chemically constrained model). In addition, all heavy atoms excluding the four equatorial CO groups were assumed to lie in a pseudosymmetry plane, and only those population parameters that obey the symmetry picking rules were refined. A radial scaling (κ') for the spherical density was refined for each atom type, together with a scaling (κ'') of the radial function for the deformation density. In addition, four sets of κ values (κ' and κ'') for the four types of chemically different C atoms [C(O), C(carbene), C(ring), and C(Me)] were refined. The κ'' parameters for the four sets of multipoles ($1 \le l \le 4$) were constrained to have the same values. The molecule was kept neutral during all refinements.

With the experimental model this procedure refined to the final κ values (the initial and final ζ values are doubled and given in $bohr^{-1}$ in square brackets), $\zeta_{final} = \kappa'' \cdot \zeta_{initial}$: $\kappa' = 1.14(1)$ and $\kappa'' = 0.97(3)$ [6.504/6.335] for Cr, $\kappa' = 1.006(2)$ and $\kappa' = 1.21(5)$ [4.472/5.432] for O, $\kappa' = 0.996(4)$ and $\kappa'' = 0.91(3)$ [3.841/3.508] for N, $\kappa' = 1.003(4)$ and $\kappa'' = 0.89(1)$ [3.176/2.817] for C(O), $\kappa' = 0.986$ (7) and $\kappa'' = 0.80(3)$ [3.176/2.533] for C(carbene), $\kappa' = 0.999(6)$ and $\kappa'' = 0.84(2)$ [3.176/2.659] for $C(sp^2)$, $\kappa' = 1.019(8)$ and $\kappa'' = 0.77(2)$ [3.176/2.453] for $C(sp^3)$, $\kappa' = 0.97(1)$ and $\kappa'' = 1.40(6)$ [2.000/2.799] for H. In addition, an isotropic extinction model (type I, dominated by mosaic spread, Lorentzian distribution of mosaic spread) based on a method proposed by Becker and Coppens[70] was applied. The mosaic spread of 13″ and domain size of 0.2 μm were obtained. The maximum amount of extinction ($y = 0.75$) is for the one, strongest reflection (011). The residual electron density map was practically featureless with the maximum and minimum values of 0.23 and −0.18 e $Å^{-3}$ (Fourier summation was obtained to a resolution of $\sin\Theta/\lambda < 0.8$ $Å^{-1}$), respectively. The final agreement factors were $R_1 = 0.0198$, $w_2R_2 = 0.0480$, and GOF = 0.80 for 327 parameters with the ratio $N_{ref}/N_{var} = 31$.

Hirshfeld's rigid bond test[71] was applied to the atomic displacement parameters obtained from the refinements. The difference between mean-square amplitudes for all bonds except for the Cr−C bonds is within the limit of 1.0×10^{-3}, proposed by Hirshfeld. The difference for the Cr−C bonds, due to the different masses of the bonded atoms, never exceeds the limit of 3.0×10^{-3} Å adopted for this bond type.[72]

ORTEP plots (Figures 1 and 12) were prepared with the program PLATON.[73a] Figures 2 and 10 were prepared using the program SCHAKAL.[73b]

Computational Details. All refinements were carried out with the full-matrix least-squares program (XDLSM) of a modified version[66a] of the XD software package;[66b] the quantity minimized was $\sum w_1(|F_{obs}| - k|F_{calc}|)^2$, where k is a scale factor. Weightings were taken as $w_1 = 1/\sigma^2(F_{obs})$ and $w_2 = 1/\sigma^2(F^2_{obs})$, and 10 151 [$F_{obs} > 3\sigma(F_{obs})$] unique reflections were used in the refinements. For the topological analysis, critical points of the electron density were searched via a Newton−Raphson algorithm implemented in XD. Properties of $\rho(\mathbf{r})$ and $\nabla^2\rho(\mathbf{r})$ were calculated after transformation of the local axis system into a global system. The experimental kinetic energy density at the BCP is estimated by $G(\mathbf{r}) = (3/10)(3\pi^2)^{2/3}\rho(\mathbf{r}_c)^{5/3} + {}^1/_6\nabla^2\rho(\mathbf{r}_c)$ as recently proposed by Abramov.[74] The potential energy density, $V(\mathbf{r})$, and the total energy density, $H(\mathbf{r}) = G(\mathbf{r}) + V(\mathbf{r})$, can be obtained by taking into account the local virial theorem,[13] ${}^1/_4\nabla^2\rho(\mathbf{r}) = 2G(\mathbf{r}) + V(\mathbf{r})$.

DFT calculations using the BPW91[75] density functional were carried out with the GAUSSIAN98[76] program suite. Unless specified otherwise, the double-ζ DZVP2 basis set[77] was our standard (denoted as I in the text), while the basis set II represents a combination of the Wachters basis set for Cr[78] along with 6-311G(d)[79] for C, N, O, and H. Because for the first-row transition metals relativistic effects have been shown to be negligible, a pseudopotential for the Cr atom was not used. All structures, except for **2**, **2a**, and **2b**, were optimized without imposing any symmetry restraints at the BPW91 level of theory. For **2a** and **2b**, minima with C_{2v} symmetry were found. The final optimized geometry of **2** has C_2 symmetry. The resulting geometries were verified to be minima by frequency calculations. Geometry optimization of acyclic chromium carbene complex **10** was terminated on the basis of negligible forces, and the following values were obtained (au): 0.000007 (max force), 0.003266 (max displacement), 0.000001 (rms force), and 0.000685 (rms displacement), with the default threshold values being 0.000450 (max force), 0.001800 (max displacement), 0.000300 (rms force), and 0.001200 (rms displacement).

Topological analysis of the theoretical electron densities was carried out using the AIMPAC software package.[80]

The average electron population of an atom is obtained by the integration of $\rho(\mathbf{r})$ over the basin of the atom, and its net charge, q, is

(66) (a) Macchi, P.; Tafipolsky, M. Modifications to XD code (see ref 66b), unpublished. (b) Koritsanszky, T.; Howard, S. T.; Su, Z.; Mallinson, P. R.; Richter, T.; Hansen, N. K. *XD, Computer Program Package for Multipole Refinement and Analysis of Electron Densities from Diffraction Data*; Free University of Berlin: Germany, June, 1997.

(67) For comparison, the new RHF ground-state atomic wave functions (STO) from both Bunge et al. [Bunge, C. F.; Barrientos, J. A.; Bunge, A. V. *At. Data Nucl. Data Tables* **1993**, *53*, 113−162] and Koga et al. [Koga, T.; Kanayama, K.; Watanabe, S.; Thakkar, A. J. *Int. J. Quantum Chem.* **1999**, *71*, 491−497] were tested, and no differences were observed in the topological parameters at the BCPs, *R*-factors, and max/min residual electron densities, deduced using the compilation of Clementi and Roetti [Clementi, E.; Roetti, C. *At. Data Nucl. Data Tables* **1974**, *14*, 177−478].

(68) Clementi, E.; Raimondi, D. L. *J. Chem. Phys.* **1963**, *38*, 2686−2689.

(69) Holladay, A.; Leung, P.; Coppens, P. *Acta Crystallogr.* **1983**, *A39*, 377−387.

(70) Becker, P.; Coppens, P. *Acta Crystallogr.* **1974**, *A30*, 129−147.

(71) (a) Harel, M.; Hirshfeld, F. L. *Acta Crystallogr.* **1975**, *B31*, 162−172. (b) Hirshfeld, F. L. *Acta Crystallogr.* **1976**, *A32*, 239−244.

(72) (a) Dunitz, J. D.; Schomaker, V.; Trueblood, K. N. *J. Phys. Chem.* **1988**, *92*, 856−867. (b) Dunitz, J. D.; Maverick, E. F.; Trueblood, K. N. *Angew. Chem.* **1988**, *100*, 910−926; *Angew. Chem., Int., Ed. Engl.* **1988**, *27*, 880−895. (c) Chandrasekhar, K.; Bürgi, H. B. *Acta Crystallogr.* **1984**, *B40*, 387−397.

(73) (a) Spek, A. L. *Acta Crystallogr.* **1990**, *A46*, C-34. (b) Keller, E. *SCHAKAL*; Crystallographic Institute: University of Freiburg, Germany, 1988.

(74) Abramov, Y. A. *Acta Crystallogr.* **1997**, *A53*, 264−272.

(75) (a) Becke, A. D. *Phys. Rev.* **1988**, *A38*, 3098−3100. (b) Perdew, J. P.; Wang, Y. *Phys. Rev.* **1992**, *B45*, 13244−13249.

(76) Frisch, M. J.; Trucks, G. W.; Schlegel, H. B.; Scuseria, G. E.; Robb, M. A.; Cheeseman, J. R.; Zakrzewski, V. G.; Montgomery, J. A., Jr.; Stratmann, R. E.; Burant, J. C.; Dapprich, S.; Millam, J. M.; Daniels, A. D.; Kudin, K. N.; Strain, M. C.; Farkas, O.; Tomasi, J.; Barone, V.; Cossi, M.; Cammi, R.; Mennucci, B.; Pomelli, C.; Adamo, C.; Clifford, S.; Ochterski, J.; Petersson, G. A.; Ayala, P. Y.; Cui, Q.; Morokuma, K.; Malick, D. K.; Rabuck, A. D.; Raghavachari, K.; Foresman, J. B.; Cioslowski, J.; Ortiz, J. V.; Stefanov, B. B.; Lui, G.; Liashenko, A.; Piskorz, P.; Komaromi, I.; Gomperts, R.; Martin, R. L.; Fox, D. J.; Keith, T.; Al-Laham, M. A.; Peng, C. Y.; Nanayakkara, A.; Gonzalez, C.; Challacombe, M.; Gill, P. M. W.; Johnson, B. G.; Chen, W.; Wong, M. W.; Andres, J. L.; Head-Gordon, M.; Replogle, E. S.; Pople, J. A. *Gaussian 98*, revision A.7; Gaussian, Inc.: Pittsburgh, PA, 1998.

(77) Godbout, N.; Salahub, D. R.; Andzelm, J.; Wimmer, E. *Can. J. Chem.* **1992**, *70*, 560−571.

(78) Wachters, A. J. H. *J. Chem. Phys.* **1970**, *52*, 1033−1036.

(79) Krishnan, R.; Binkley, J. S.; Seeger, R.; Pople, J. A. *J. Chem. Phys.* **1980**, *72*, 650−654.

(80) (a) Biegler-König, F. W.; Bader, R. F. W.; Tang, T. *J. Comput. Chem.* **1982**, *3*, 317−328. (b) Cheeseman, J. R.; Keith, T. A.; Bader, R. F. W. AIMPAC program package; McMaster University, Ontario, Canada, 1994.

given by the difference between the nuclear charge and the electron population. Calculation of the atomic properties reported here is accomplished with the program PROAIMV[81] from AIMPAC software package.[80]

The search for critical points in the *negative* Laplacian of the experimental electron density, $-\nabla^2\rho(\mathbf{r}_c)$, was performed with the help of the Newton−Raphson method implemented in the XDPROP program by one of us (M.T.). The same algorithm is used in the BUBBLE program (written by P. Krug, 1990) of the AIMPAC suite of programs.[80] A more robust algorithm as implemented in the TOPXD program[82] is used to check the properties of the critical points in the *negative* Laplacian of the experimental electron density. The electron localization function (ELF)[50] was calculated with the TopMod suite of programs.[83] All contour plots were produced using the programs written in our lab. All 3-D isovalue surface plots were prepared with XDGRAPH from XD software package.[66b]

X-ray Structure Analysis of 2. Compound **2** crystallizes as yellow rhombuses with two independent molecules in the asymmetric unit. Formula: $C_{10}H_8CrN_2O_5$; $M_r = 288.18$; 0.06 × 0.12 × 0.12 mm^3; $a = 13.2440(3)$ Å, $b = 10.5510(2)$ Å, $c = 18.1170(3)$ Å, $\beta = 106.538(1)°$, $V = 2426.89(9)$ Å^3; monoclinic; space group *Ia* (No. 9); $Z = 8$; $F(000) = 1168$; $D_{calc} = 1.577$ g/cm^3; $\mu = 0.96$ mm^{-1}; $\lambda = 0.71073$ Å (Mo Kα); Nonius Kappa-CCD system; $T = 173(1)$ K; ω- and ϕ-scans with $\Delta\phi = \Delta\omega = 2°$; empirical absorption correction[63] applied ($T_{min} = 0.899(3)$, $T_{max} = 0.944(3)$); 5567 unique reflections collected; $4.6° < 2\Theta < 55.0°$; $R_{int}(F_o^2) = 0.0355$; 5421 observed reflections [$I > 2\sigma(I)$]; 325 refined parameters (refinement on F_o^2); $R_1 = 0.0239$, $wR_2 = 0.0566$; GOF = 1.07; max/min residual electron density, 0.23/−0.22 e Å^{-3}; Flack parameter, 0.00(1); hydrogen atoms on calculated positions.[84]

X-ray Structure Analysis of 10. Compound **10** crystallizes as dark yellow prisms. Formula: $C_{17}H_{28}CrN_2O_4$; $M_r = 376.41$; 0.12 × 0.12 × 0.40 mm^3; $a = 8.1983(1)$ Å, $b = 12.5454(1)$ Å, $c = 18.9873(1)$ Å, $V = 1952.86(3)$ Å^3; orthorhombic; space group $P2_12_12_1$ (No. 19); $Z = 4$; $F(000) = 800$; D_{calc}=1.280 g/cm^3; $\mu = 0.607$ mm^{-1}; $\lambda = 0.71073$ Å (Mo Kα); Nonius Kappa-CCD system; $T = 173(1)$ K; ω- and ϕ-scans with $\Delta\phi = \Delta\omega = 2°$; empirical absorption correction[63] applied [$T_{min} = 0.885(2)$, $T_{max} = 0.933(2)$]; 4482 unique reflections collected; $4.0° < 2\Theta < 55.0°$; $R_{int}(F_o^2) = 0.0308$; 4244 observed reflections [$I > 2\sigma(I)$]; 330 refined parameters (refinement on F_o^2); $R_1 = 0.0240$, $wR_2 = 0.0595$; GOF = 1.04; max/min residual electron density, 0.17/−0.32 e Å^{-3}; Flack parameter, 0.00(1); hydrogen atoms were refined isotropically.[84]

Acknowledgment. This work was supported by the Deutsche Forschungsgemeinschaft and the Alexander von Humboldt Foundation (through a Postdoctoral Fellowship to M.T.). We thank Prof. Vladimir Tsirelson and Prof. Pierro Macchi for help and fruitful discussions and the referees for useful comments.

Supporting Information Available: Calculated nucleus-independent chemical shifts for **1**, **1a**, **1b**, **2**, **2a**, and **2b**, atomic charges and quadrupole moments, tables of crystal data, structure solution and refinement, atomic coordinates, bond lengths and angles, anisotropic thermal parameters and residual electron density maps for **1** and **2**, and multipole parameters for **1**. Tables comparing the results of several multipoles, definition of local coordinate systems for **1**, and deformation and residual density maps. Results of the fully optimized geometry (C_2 symmetry), NPA, topological parameters, atomic charges, and quadrupole moments, and bond ellipticity profiles for further model systems such as 1,2-dimethylpyrazol-4-ylidene (PDF). X-ray crystallographic data for **1**, **2**, and **10** in CIF format are also available. This material is available free of charge via the Internet at http://pubs.acs.org.

JA011761K

(81) Keith, T. A. Ph.D. Thesis, McMaster University, Ontario, Canada, 1993.
(82) Volkov, A.; Gatti, C.; Abramov, Yu.; Coppens, P. *Acta Crystallogr*. **2000**, *A56*, 252−258.
(83) Noury, S.; Krokidis, X.; Fuster, F.; Silvi, B. TopMod Package, Paris, 1997.
(84) Sheldrick, G. M. SHELXL97. Program for crystal structure refinement; University of Göttingen, Germany, 1997.